Arabian Journal of Chemistry (2023) **16**, 104988

King Saud University

Arabian Journal of Chemistry

www.ksu.edu.sa
www.sciencedirect.com

ORIGINAL ARTICLE

Experimental assessment and molecular-level exploration of the mechanism of action of Nettle (*Urtica dioica* L.) plant extract as an eco-friendly corrosion inhibitor for X38 mild steel in sulfuric acidic medium

Radouane Maizia [a], Aida Zaabar [a,b], Atmane Djermoune [c,d], Damia Amoura [a], Serguei Martemianov [e], Anthony Thomas [e], Awad A. Alrashdi [f], Laid Makhloufi [a], Hassane Lgaz [g,*], Abdelhafid Dib [a], Maryam Chafiq [h,*], Young Gun Ko [h,*]

[a] *Laboratoire d'Electrochimie, Corrosion et de Valorisation Energétique (LECVE), Faculté de Technologie, Université de Bejaia, 06000 Bejaia, Algeria*
[b] *Département de Génie des Procédés, Pôle Technologique, Université de Bouira, 10000 Bouira, Algeria*
[c] *Department de genie mécanique, Laboratoire de Mécanique, Matériaux & Energetique, Université de Bejaia, Algeria*
[d] *Centre de Recherche Scientifique et Technique en Analyses Physico-Chimiques (CRAPC), Algeria*
[e] *Institut Pprime, Université de Poitiers-CNRS-ENSMA, UPR 3346, 2 Rue Pierre Brousse, Batiment B25, TSA 41105, 86073 Poitiers Cedex 9, France*
[f] *Chemistry Department, Umm Al-Qura University, Al-Qunfudah University College, Saudi Arabia*
[g] *Innovative Durable Building and Infrastructure Research Center, Center for Creative Convergence Education, Hanyang University ERICA, 55 Hanyangdaehak-ro, Sangrok-gu, Ansan-si, Gyeonggi-do, 15588, Republic of Korea*
[h] *Materials Electrochemistry Group, School of Materials Science and Engineering, Yeungnam University, Gyeongsan 38541, South Korea*

Received 24 March 2023; accepted 8 May 2023
Available online 12 May 2023

KEYWORDS

Nettle extract;
Green inhibitor;
Mild steel;
Corrosion inhibition;
Density-functional tight-binding;
Density of states

Abstract The development of green corrosion inhibitors has gained considerable importance in recent years due to their minimal environmental impact and sustainable nature. As industries increasingly seek eco-friendly alternatives to conventional corrosion inhibitors, research focused on identifying effective and renewable corrosion protection solutions becomes imperative. The main purpose of this study is to evaluate the inhibition action of Nettle extract (NE) (*Urtica dioica* L.) as a promising green corrosion inhibitor for mild steel in a 0.5 mol/L H_2SO_4 medium. In this work, the corrosion protection performance of NE was assessed using weight loss, electrochemical, surface characterization, and computational chemistry methods. The results indicated that NE acted as an effective corrosion inhibitor, with inhibition efficiency reaching a maximum of 90% at a concen-

* Corresponding authors.
E-mail addresses: hlgaz@hanyang.ac.kr (H. Lgaz), maryam.chafiq@yu.ac.kr (M. Chafiq), younggun@ynu.ac.kr (Y.G. Ko).

https://doi.org/10.1016/j.arabjc.2023.104988

tration of 4 g L^{-1}. Polarization studies revealed that NE functions as a mixed-type inhibitor, while electrochemical impedance spectroscopy (EIS) results showed an increase in charge transfer resistance and a decrease in double layer capacitance values in the presence of NE. Surface characterization analysis confirmed the formation of a protective NE layer on the steel surface. Furthermore, Density-functional tight-binding (DFTB) simulations identified Quercetin, Kaempferol, and Serotonin as having stronger chemical bonding with the Fe(1 1 0) surface, while Histamine molecules exhibited physical interactions with iron atoms. This comprehensive evaluation of NE's inhibition action not only supports its potential as an eco-friendly inhibitor for mild steel corrosion protection but also contributes to the development of sustainable corrosion control strategies.

1. Introduction

Corrosion is commonly defined as degradation of a metallic material by its physico-chemical interaction with the environment that adversely affects its properties and applications and leads to numerous safety and economic losses, (Verma et al., 2017a; Verma et al., 2017b). The economic losses caused by corrosion are now enormous, estimated by the National Association of Corrosion Engineers (NACE) to be in the range of 1–5% of an industrialized country's gross national product, particularly in countries such as China, USA, Japan, and Germany etc.(Verma et al., 2017b; Sedik et al., 2020). Mild steel is extensively utilized in civil construction, agriculture, maritime and industrial applications (oil refineries, petrochemical industry, packaging) due to its advantages such as good mechanical resistance, low cost, availability, high ductility, adjustable surface and hardness etc., (Sedik et al., 2020; Haddadi et al., 2019). On the other hand, acidic solutions are broadly used in industry for cleaning, pickling, acidizing oil wells and removing deposits (rusts and scales) (Haddadi et al., 2019)-(Ehsani et al., 2017). Because of the aggressiveness of these acid solutions, corrosion inhibitors must be used to protect and extend the life of metallic equipment.

Nowadays, the usage of many synthetic inhibitors (organic and inorganic inhibitors) has been severely restricted and limited due to their high cost, bioaccumulation, and toxicity to the environment and human health (Sedik et al., 2020; Dehghani et al., 2020a; Berrissoul et al., 2020). In this context, the trend toward the development and usage of green inhibitors that are environmentally acceptable, and biodegradable is motivating many researchers. Green inhibitors are rich sources of chemical compounds that can be extracted by simple low-cost procedures from natural products such as medicinal plants, heartwood, roots, leaves, bark, seeds and fruits (Saeed et al., 2019; Gerengi et al., 2016). These extracts contain complex organic groups such as tannins, alkaloids, nitrogenous bases, carbohydrates, amino acids and flavonoids (Verma et al., 2018; Zaabar et al., 2021).

There have been several studies, on the use of extracts, as green corrosion inhibitors to preserve mild steel in acidic environments such as: Dardagan Fruit from *Bingöl* (Sedik et al., 2020), *Diospyros kaki* leaves (Gerengi et al., 2016), Aloe Vera leaf (Mehdipour et al., 2015), *Lavandula Mairei* (Berrissoul et al., 2020), *Malva sylvestris* (Tehrani et al., 2021), aquatic artichoke (Salmasifar et al., 2021), *liriope platyphylla* (Chung et al., 2021), oat (Zaabar et al., 2021), *Peganum harmala* seed (Bahlakeh et al., 2019), *Ziziphora* leaves (Dehghani et al., 2020a), *Thymus vulgaris* (Ehsani et al., 2017), *Tamarindus indiaca* (Dehghani et al., 2019a), *Ircinia strobilina* (Fernandes et al., 2019a), *Saraca asoca* among others (Saxena et al., 2018), Nettle extract in NaCl medium (Izadi et al., 2018). To our knowledge, no research has been published on the inhibitory characteristics of nettle extract (NE) on mild steel corrosion in the H_2SO_4 medium. Nettle (*Urtica dioica* L.), often known as stinging nettle, is a perennial plant that thrives in temperate and tropical regions all over the world. It grows 2 to 4 m tall and has pointed leaves and white to yellowish flowers (Rajput et al., 2018). The chemical components of NE are flavonoids, tannins, volatile compounds, polysaccharides, sterols, isolectins, terpenes, fatty acids, protein, minerals and vitamins. They contain electronegative functional groups (C═O, N─H, O─H and C═S) and multiple carbon–carbon bonds (C═C and C─C) that potentially facilitate the inhibition process by adsorbing on metal surfaces (Zaabar et al., 2014; Di Virgilio et al., 2015).

The aim of this paper is to investigate the potential of Nettle (*Urtica dioica* L.) as a green and sustainable corrosion inhibitor for mild steel in sulfuric acid solutions. With the ever-increasing demand for environmentally friendly alternatives to conventional corrosion inhibitors, the exploration of Nettle, a renewable and biodegradable resource, serves as a significant contribution to the field of corrosion prevention. The study focuses on evaluating the effectiveness of Nettle extract in mitigating corrosion, understanding the underlying inhibition mechanisms, and identifying key active components responsible for the inhibition process. To this end, different chemical and electrochemical methods such as weight loss, potentiodynamic polarization curves, electrochemical impedance spectroscopy and electrochemical potential noise assessments were carried out. The morphology and composition of the metal surface were investigated using contact angle, X-ray diffraction, and optical microscopy analyses. Besides, the electronic and reactivity of four NE's components were discussed using quantum chemical calculations. To get deep insights into the adsorption mechanism of the four NE components (Quercetin, Kaempferol, Serotonin, Histamine) on the steel surface, DFTB simulations were performed. The most stable adsorption geometries and projected density of states were used to analysis the interaction mechanisms between NE components and Fe(1 1 0) surface. By establishing a detailed characterization of Nettle's anti-corrosion performance, this research will not only pave the way for the development of an eco-friendly corrosion protection material but also promote the use of sustainable chemicals, thereby reducing the environmen-

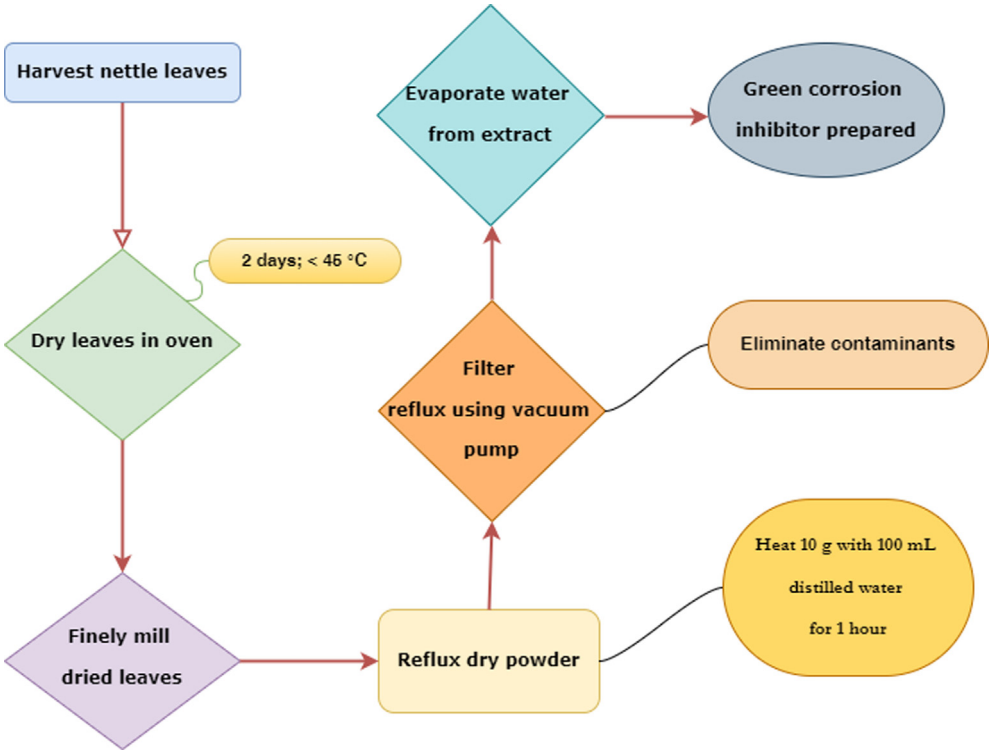

Scheme 1 A flowchart of the preparation procedure of NE extract inhibitor.

tal impact associated with the use of hazardous corrosion inhibitors.

2. Experimental procedure

2.1. Preparation of plant extract

The nettle leaf extract was selected as corrosion inhibitor for several reasons such as its huge and widespread availability, low cost, eco-friendly and safe to living organism properties. The leaves of the nettle plant harvested were immediately put to dry in an oven not exceeding 45 °C for two days to eliminate any trace of water. It was finely milled after drying to produce a uniform powder. The extract was prepared in water using the reflux technique, which involves heating 10 g of dry powder with 100 mL of distilled water for one hour. The reflux is then filtered using a vacuum pump to eliminate any contaminants (Zaabar et al., 2021; Abdel-Gaber et al., 2006; Zaabar et al., 2019). Finally, the extract was prepared by evaporating the water (See Scheme 1). The inhibition efficiency of the NE was evaluated at several concentrations ranging from 0.4 to 6 g L^{-1} (Quraishi et al., 2010). All chemicals were used as received without further purification.

2.2. Solutions and electrodes

The 0.5 mol/L H_2SO_4 solution was prepared and used as testing electrolyte by the dilution of analytic grade H_2SO_4 (95–98% H_2SO_4; Sigma-Aldrich). All experiments were performed in the 100 mL solution of test electrolyte. Mild steel of the following composition was employed as working electrode for the experimental studies: 98% Fe, 0.94% Mn, 0.31% Si, 0.2% C and less than 1% Al. For weight loss study, working electrode specimens of 3 cm × 2.1 cm × 0.1 cm were taken. The electrochemical studies were performed on mild steel as a working electrode with an exposed area of 0.785 cm^2. Before performing the experiments, mild steel surfaces were cleaned using emery paper of different grades (120–2400 μm), followed by washing with deionized water, acetone (Sigma-Aldrich) and drying using hot air blower.

2.3. Measurement techniques

2.3.1. Weight loss measurements

Mild steel samples, which have already been prepared and weighed, were immersed in 0.5 mol/L H_2SO_4 at room temperature, with and without varying dosages of NE. The steel samples were then removed and cleaned with distilled water, after every 24 h of immersion. Then cleaned to remove corrosion products from the metal surface. The sample was then weighed after being rinsed with distilled water and dried. The mass loss was monitored for 21 days and the inhibitory efficiency (*IE*) was calculated by Eq. (1) (Dehghani et al., 2019a; Fadhil et al., 2020):

$$IE(\%) = \left(\frac{w - w_i}{w}\right) \times 100 \quad (1)$$

Where w and w_i represent the mass loss of the specimens after immersion, without and with inhibitor, respectively.

2.3.2. Electrochemical measurements

To perform electrochemical measurements, a classical setup consisting of a single compartment glass cell and three electrodes system was used. The system composed of a reference

electrode (saturated calomel (SCE)), a counter electrode made of a platinum grid with a large surface area and a working electrode made of mild steel employing AUTOLAB® potentiostat/galvaostat (PGSTAT30, Ecochemie, Netherlands) controlled by Nova® software. The intensity-potential curves were obtained in potentiodynamic mode. The potential applied to the sample varied continuously, with a scan rate of 1 mV s^{-1} in the potential range of −1000 to −500 mV.

The inhibition efficiency $IE(\%)$ is calculated using the following formula (Singh et al., 2020):

$$IE(\%) = \left(\frac{i^0_{corr} - i_{corr}}{i^0_{corr}}\right) \times 100 \quad (2)$$

Where i^0_{corr} and i_{corr} are the corrosion current densities, without and with NE inhibitor, respectively.

Electrochemical impedance spectroscopy (EIS) plots were obtained at a corrosion potential with a frequency range of 100 kHz-10 mHz and an amplitude of 10 mV. The $IE(\%)$ is calculated using the following expression (Ehsani et al., 2017):

$$IE(\%) = \left(\frac{R_{ct} - R^0_{ct}}{R_{ct}}\right) \times 100 \quad (3)$$

Where R_{ct} and R^0_{ct} represent the charge transfer resistances in the presence and absence of the NE inhibitor, respectively.

The formula for calculating the double layer capacitance (C_{dl}) is as follows (Zaabar et al., 2021):

$$C_{dl} = \frac{1}{2\pi f_m R_{ct}} \quad (4)$$

Where f_m is determined at the maximum imaginary part (Im $(Z)_{max}$).

Electrochemical potential noise (EPN) analyses were carried out by an AUTOLAB® (PGSTAT30, Ecochemie, Netherlands) controlled by NOVA® software. The experimental implementation of this technique requires isolating the system (the electrochemical cell) from external electromagnetic interference signals. For this purpose, a Faraday cage was used to isolate the test cell (Mehdipour et al., 2015; Ehsani et al., 2017). The duration of each EPN measurement was set to 2000 s and with sampling frequency of 10 Hz. For the collection of EPN data, direct potential (DC) component was firstly eliminated from the raw signal using the five-order polynomial fitting a frequently used method in DC removal (Ma et al., 2017; Bertocci et al., 2002).

The way of dealing with electrochemical noise (EN) measurements is based on several techniques, namely spectral analysis (Fast Fourier transform), statistical analysis (higher order moments) and temporal-frequential analysis (wavelets). This work is limited to spectral analysis in the frequency domain (Power spectral density) and statistical analysis in the time domain (standard deviation (STD), Skewness (SK) and Kurtosis (KU)), which is more appropriate for possible practical applications. All calculations of signal processing were carried out using MATLAB® software.

2.4. Surface analysis

2.4.1. FT-IR analysis

In order to detect the presence of different functional groups in Nettle leaves extract, FT-IR tests were employed. The FT-IR spectrum was recorded between 400 and 4000 cm^{-1} using a Shimadzu FT-IR spectrophotometer (Testscan Shimadzu FT-IR 8000 series).

2.4.2. Contact angle

The contact angle measurements were made by a sessile drop technique. For this, 6 μL of distilled water was dropped on the samples of mild steel using a micro syringe and photographed with a black and white CCD camera. The contact angle was measured automatically by ADVANCE® software. To obtain reliable contact angle data, three droplets were dropped at different regions of the surface of the electrode and the mean value was calculated.

2.4.3. X-ray diffraction (XRD) analysis

X-ray diffraction is one of the most common methods for determining the nature of the compounds produced on the electrode surface. Mild steel samples were examined using a Panalytical Empyrean® diffractometer (XRD, Empyrean-100, Dutch PANalytical Company) after immersion in 0.5 mol/L H_2SO_4 solution for 24 h without and with the optimum concentration (4 g L^{-1}) of NE inhibitor.

2.4.4. Optical microscopy characterization

The steel samples were exposed to a sulfuric acid solution (0.5 mol/L) without and with 4 g L^{-1} of NE for three hours. All samples were removed and washed with distilled water. In addition, they were dried at room temperature. Finally, the samples were examined before and after immersion with a Zwick ZHV10® metallurgical microscope using (Zwick Roell, Germany) testX'pert® analytical software.

2.5. Quantum chemical calculations

Density functional theory (DFT) was used to perform the quantum chemical calculations of the four major NE components (histamine, serotonin, quercetin, and kaempferol). All compounds were optimized using B3LYP linked at the 6–31 g (d, p) level of theory in liquid phase (water) using the conductor polarizable computational model (CPCM) (Cossi et al., 2003; Takano and Houk, 2005). Gaussian09 and its graphical interface GaussView® software were used to calculate all quantum chemical parameters (Dennington et al., 2016; Frisch et al., 2016).

The theoretical parameters were obtained using the following equations (Abdallah et al., 2021) (Chafiq et al., 2020):

$$\text{Energy gap}: \Delta E = E_{LUMO} - E_{HOMO} \quad (5)$$

Where: E_{LUMO} and E_{HOMO}, are the energies of the lowest empty molecular orbital and the highest occupied molecular orbital, respectively.

$$\text{Absolute electronegativity}: \chi = \frac{I + A}{2} \quad (6)$$

$$\text{Global hardness}: \eta = \frac{I - A}{2} \quad (7)$$

$$\text{Global softness}: \sigma = \frac{1}{\eta} \quad (8)$$

$$\text{Fraction of transferring electrons}: \Delta N = \frac{\phi - \chi_{inh}}{2(\eta_{Fe} + \eta_{inh})} \quad (9)$$

where, ϕ (the work function of iron) equal to 4.82 eV (Abdallah et al., 2021; Dehghani et al., 2019b) η_{Fe} = 0,- $I = -E_{HOMO}$ and $A = -E_{LUMO}$ are the ionization potential and the electron affinity, respectively.

2.6. Density-functional tight-binding (DFTB)

For deeper insights into the interactions between NE's components, i.e., quercetin, kaempferol, serotonin and histamine, and the iron surface, density-functional based tight-binding (DFTB) method has been used. The SCC-DFTB method is an approximation that assumes a second-order expansion of the Kohn–Sham Density Functional Theory. Its accuracy in predicting structural and electronic properties is like first-principles calculations, but it is ~100–1000 times faster as well as suitable for large systems. Herein, the inhibitor-iron interactions were fully optimized by spin polarized SCC-DFTB, including dispersion interaction with Slater-Koster trans3d using the DFTB + code (Hourahine et al., 2020). The generalized gradient approximation (GGA) within its PBE formulation was used for the electron exchange and correlation (Perdew et al., 1996). The adsorption systems were fully optimized using a SCC tolerance of 10^{-8} au, thermal smearing (Methfessel-Paxton smearing distribution function), and Broyden mixing scheme. All other convergence tolerance values were set according to fine quality. Meanwhile, the bulk lattice parameters optimization was carried out using (8x8x8) k-point grid, which was reduced to (2x2x1) k-point grid for adsorption models.

The optimization of bulk lattice parameters reproduced a value of 2.848 Å, which is close to the experimental one of 2.862 Å, confirming the accuracy of selected parameters. Inhibitor-iron adsorption models were generated by constructing Fe(1 1 0) iron surface consisting of a (5x5) supercell and a vacuum spacing of 20 Å along the z-direction separating periodic image in each direction. Then, inhibitor molecules were placed on the top side of the slab and all atoms were allowed to relax except the two bottom-most atomic layers. SCC-DFTB optimization of standalone molecules was carried out by constructing a cubic box of 30 Å in size. The interaction energy was used as a main parameter to estimate the adsorption strength of molecules, which is calculated according to the following equation (Lgaz and Lee, 2022):

$$E_{\text{inter}} = E_{\text{mol/surf}} - (E_{\text{mol}} + E_{\text{surf}}) \quad (10)$$

Where E_{mol}, E_{surf}, and $E_{\text{mol/surf}}$ denote the total energies of isolated molecules, Fe(1 1 0) iron surface, and molecule/Fe (1 1 0) adsorption systems.

3. Results and discussion

3.1. FTIR analysis

FT-IR analysis was conducted to verify the presence of several functional groups that exist in the extract of *Nettle* plant. The FT-IR spectrum is depicted in Fig. 1. In these spectra, a significant broad peak appeared at 3390 cm^{-1}, which is attributed to the stretching vibration of the O—H or N—H bonds. The

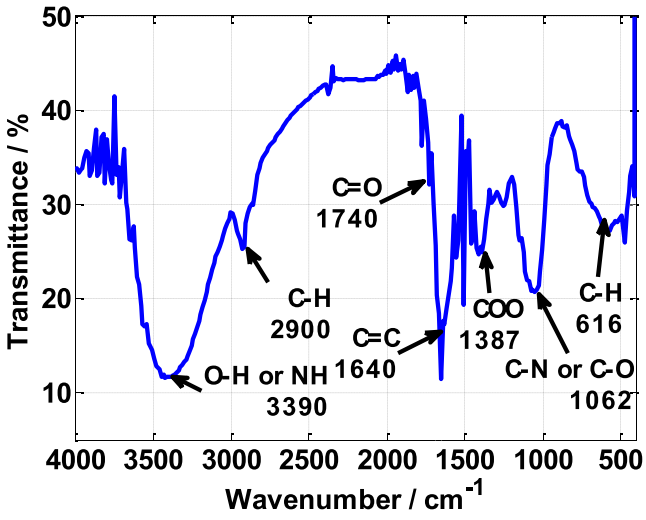

Fig. 1 FT-IR spectra of Nettle extract powder.

2900 cm^{-1} peak is due to the stretching vibration of C—H bond. Also, the 1740 cm^{-1} peak shows the presence of C═O bond and the peak at 1640 cm^{-1} is attribute to double C═C bond of aromatic benzene rings (Dehghani et al., 2019b). The peak appearing at 1062 cm^{-1} is due to the stretching vibration of the C—N or C—O bond. Finally, the absorption peaks below 1000 cm^{-1} can be due to C—H vibration of benzene rings present in the NE extract (Tan et al., 2021). Therefore, the presence of diverse functional groups such as multiple bonds, aromatic rings, and heteroatoms (O, N) can enhance the adsorption process and minimize the corrosion rate (de Britto Policarpi and Spinelli, 2020).

By consulting the literature (Keramatinia et al., 2019) and combined with FT-IR analysis, it can be concluded that the molecular formulas of the main chemical components in NE are histamine, serotonin, quercetin, and kaempferol. These molecules possess multiple bonds, aromatic rings, and heteroatoms (O). Therefore, they can interact with the metal surface using donor–acceptor mechanism to form a protective layer at the interface carbon steel/solution.

3.2. Weight loss measurements

Weight loss is a simple method to implement and does not require a lot of equipment. In addition, it is considered as the first approach for determining the rate of corrosion and the corrosion inhibition *(IE)* of an inhibitor. Fig. 2**a** illustrates the weight loss of mild steel in the sulfuric acid medium over time, in absence and in the presence of various concentrations of NE at room temperature. From Fig. 2**a**, it is clear that the mass loss decreases with the increase of the NE inhibitor concentration and from C ≥ 2 g L^{-1} the mass loss remains almost invariable with time. Thus, the mass loss is largely superior in the blank solution compared to the presence of NE ($\Delta m_{withoutNE} = 35 \times \Delta m_{withNE}$). This phenomenon is mostly due to NE inhibitor adsorption on the steel surface, which inhibits the mild steel from dissolving.

The variation of inhibition efficiency (*IE*) with NE concentrations is shown in Fig. 2**b**. It can be clearly seen that the inhibition efficiency of NE increases with its concentration and a maximum efficiency of 95% is achieved at 4 g L^{-1} concentra-

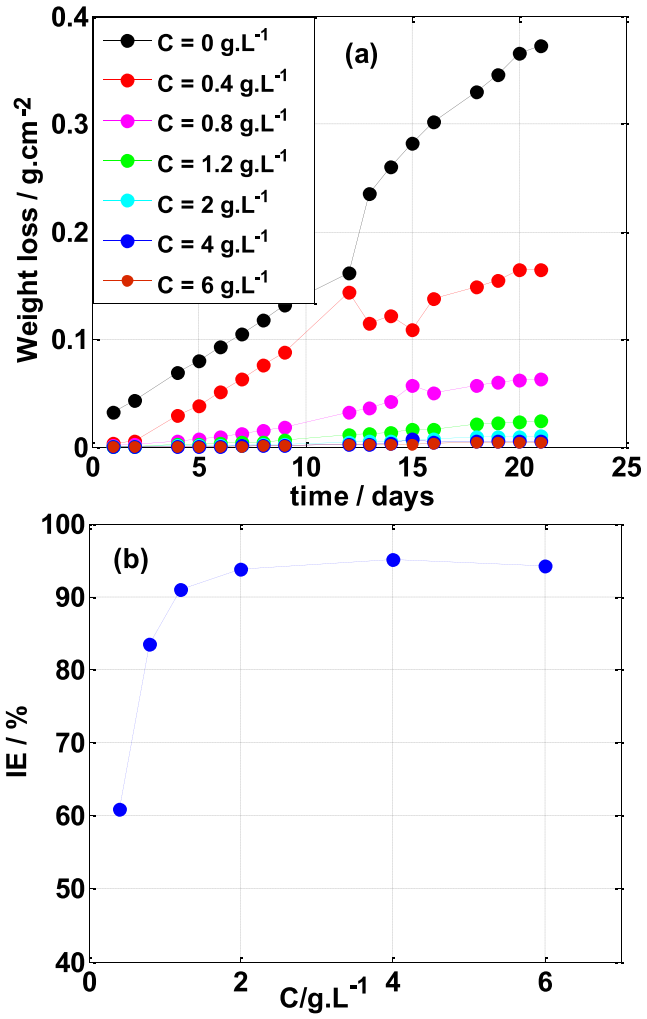

Fig. 2 **(a)** Weight loss-time curves for mild steel in 0.5 M H_2SO_4 solution without and with different concentrations of NE and **(b)** inhibition efficiency vs concentration of NE, with immersion time of one day.

tion. The phytochemicals present in the NE prevent metal dissolution by creating a protective layer on the working electrode surface (Fernandes et al., 2019a; Haruna et al., 2018).

3.3. Potentiodynamic polarization curves (PPCs)

Fig. 3 shows the PPCs (I vs E) for mild steel dissolution in sulfuric acid medium (0.5 mol/L), without and with NE at 25 °C. As per the literature reports, polarization studies give information about mechanism of corrosion and possible mechanism of corrosion inhibition process (Fernandes et al., 2019b). From Fig. 3, it can be clearly observed that in the absence and presence of NE, the shape of polarization curves is similar which indicates that mild steel corrosion mechanism does not change in the presence of NE, though the corrosion current densities for anodic as well as cathodic curves are greatly reduced in the presence of NE. The decrease of anodic and cathodic current densities suggests that NE becomes effective by adsorbing its active phytochemicals on the surface of the metal, blocking the active sites responsible for corrosion.

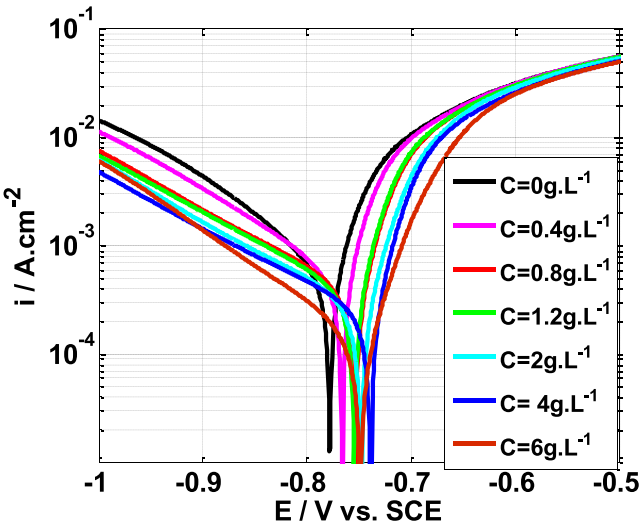

Fig. 3 Polarization curves of mild steel in 0.5 M H_2SO_4 solution without and with various concentrations of NE at scan rate of 1 $mV.s^{-1}$ and T = 25 °C.

Table 1 represents the electrochemical polarization parameters derived from extrapolation of the linear segments of Tafel curves.

Table 1 shows that when the NE concentration increases, the corrosion potential (E_{corr}) shifts to more positive (noble) potentials. According to the literature, if the E_{corr} values shift more than |85| mV from the blank, the inhibitor can be classified as cathodic (E_{corr} shifts by −85 mV) or anodic (E_{corr} shifts by + 85 mV), but if the E_{corr} values shift less than 85 mV from the blank, the inhibitor can be classified as mixed type (Fernandes et al., 2019a; Bentrah et al., 2014; Chaitra et al., 2015). The highest displacement measured in this research is 40 mV, indicating that NE acts as a mixed-type inhibitor.

Furthermore, adding the NE inhibitor changed the values of cathodic Tafel slopes (β_c), suggesting that NE has an effect on hydrogen evolution kinetics (change of the mechanism of the cathodic reaction). As a result, NE has a substantial inhibitory effect on mild steel corrosion (Dehghani et al., 2020b; Xavier Stango and Vijayalakshmi, 2018). The addition of the inhibitor NE also affected the values of the anodic slopes (β_a), which might be due to extract molecules adsorption on anodic sites of mild steel (Dehghani et al., 2020a; Li et al., 2007; Dehghani et al., 2020b; Dehghani et al., 2019c). In addition, it can be observed that when the NE inhibitor concentration rises, the inhibitory efficiency (IE) rises with it, reaching a maximum of 90% at a concentration of 4 g L^{-1}. The findings of this method show that NE extract is an excellent mild steel inhibitor in the sulfuric acid media.

3.4. Electrochemical impedance measurements

The electrochemical impedance is a very powerful method to characterize the solid/electrolyte interface. It has been extensively utilized in corrosion inhibition studies (Mehdipour et al., 2015; Ehsani et al., 2017; Zaabar et al., 2014; Abdel-Gaber et al., 2006; Quraishi et al., 2010). Fig. 4 highlights the Nyquist plots of mild steel samples immersed in sulfuric acid medium (0.5 mol/L) without and with different concentra-

Table 1 Electrochemical kinetic parameters and inhibition efficiency obtained with polarization measurements of mild steel electrode in 0.5 M H_2SO_4 solution in the absence and presence of different concentrations of NE.

Concentration (g L^{-1})	i_{corr} (mA cm^{-2})	E_{corr} (mV_{ESS})	$-\beta_c$ (mV dec^{-1})	β_a (mV dec^{-1})	R_p (Ohm cm^2)	IE(%)
0	0.797	− 778.69	266.22	107.29	41.72	–
0.4	0.518	− 767.17	259.89	77.73	50.22	35.01
0.8	0.346	− 754.31	254.90	66.60	66.35	56.59
1.2	0.158	− 752.59	203.07	38.97	89.97	80.18
2.0	0.100	− 747.79	188.29	40.50	144.92	87.45
4.0	0.081	− 739.73	196.35	34.17	156.23	89.84
6.0	0.142	− 747.79	207.87	64.14	155.13	82.18

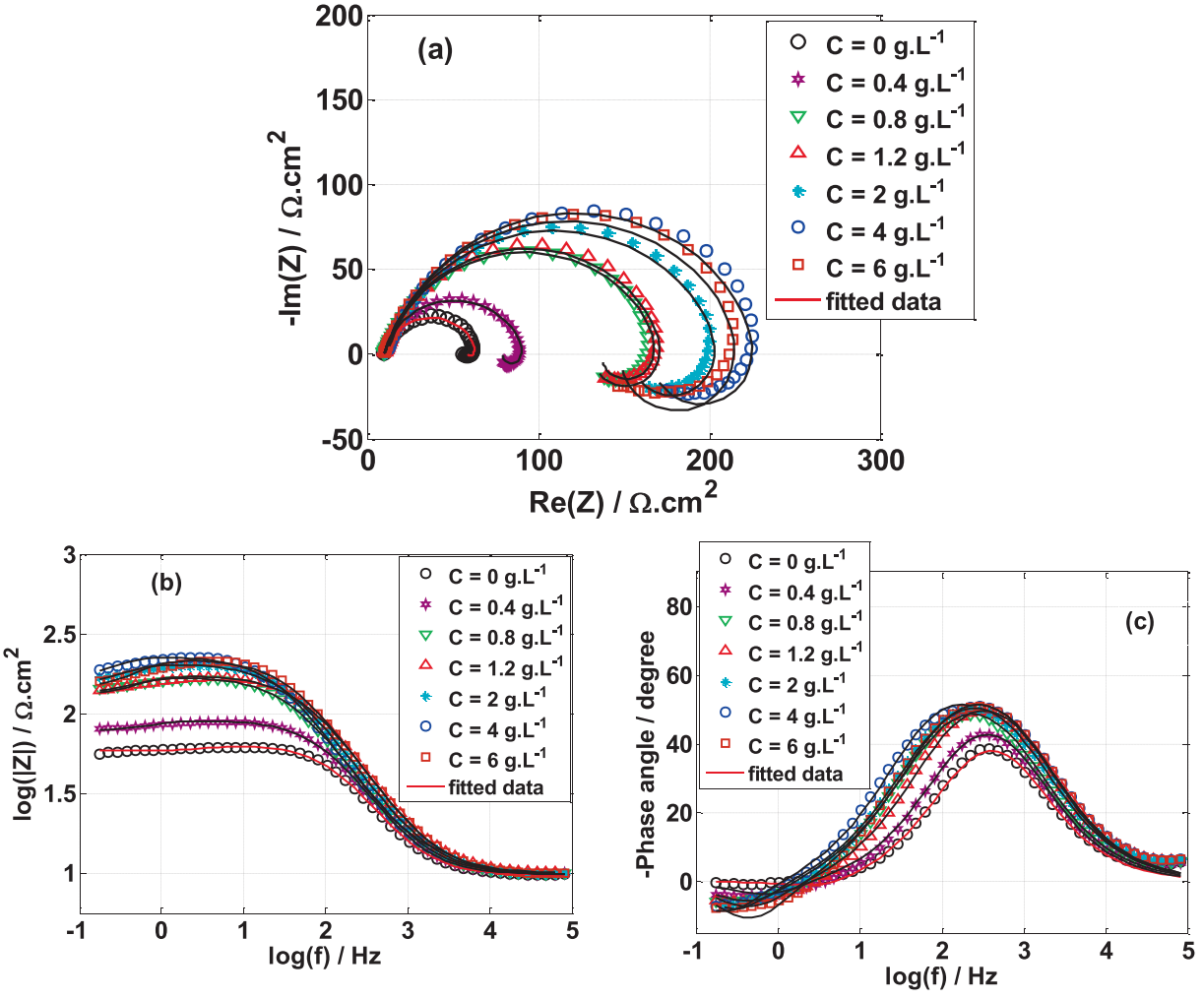

Fig. 4 Nyquist plots for mild steel in 0.5 M H_2SO_4 solution without and with different concentrations of Nettle extract at E_{ocp} and T = 25 °C.

tions of NE inhibitor at open circuit potential (E_{ocp}) and T = 25 °C. All impedance spectra have the same shape, each spectrum is featured by a single capacitive loop at high frequencies and an inductive loop at low frequencies range.

The capactive loop appeared at high frequencies is due to the charge transfer process and the double layer capacitance generated at the solid/liquid interface (mild steel/solution) (Gerengi et al., 2016; Markhali et al., 2013). In the absence of NE, the inductive loop can be related to the adsorption of the species such as $(SO_4^{-2})_{ads}$ and $(H^+)_{ads}$ on the electrode surface (Ahamad et al., 2010; Yeganeh et al., 2020; de Britto Policarpi and Spinelli, 2020). However, in the presence of NE, the inductive loop is more prominent which might be related to the adsorption of NE molecules on the steel surface.

According to Nyquist plots, the size of the semicircles (capacitive loops) increases when NE is added to the H_2SO_4 solution, and the maximal diameter was found for 4 g $L^{-1}$of NE (optimal concentration). This indicates an increased charge transfer resistance (R_{ct}), which is consistent with the literature (Zaabar et al., 2021; Zaabar et al., 2014; de Britto Policarpi and Spinelli, 2020; Ashassi-Sorkhabi and Asghari, 2008). The increase in resistance (R_{ct}) caused by increasing NE concentration indicates significant adsorption of NE molecules on the metal surface, suggesting efficient electrode surface blocking (Sedik et al., 2020; Yeganeh et al., 2020).

The impedance data were analyzed using ZsimpWin® plot software and fitted by electrical circuit presented in Fig. 5. These equivalent circuits are extensively reported in the literature (Sedik et al., 2020; Danaee et al., 2019; Khadraoui et al., 2016). The elements related to this circuit consist of:(R_e) represents electrolyte resistance, (R_{ct}) represents charge transfer resistance, (CPE) represents constant phase element; the CPE was chosen to replace the pure capacitor because of the electrode surface's heterogeneities (Rabizadeh and Asl, 2019). The inductance element is (L), while the inductive resistance is (R_L).

The impedance parameters obtained by fitting electrochemical data using an appropriate equivalent circuit are shown in Table 2.

Table 2 shows that the addition of the NE inhibitor leads to a significant improvement in charge transfer resistance (R_{ct}), indicating that the anticorrosive effectiveness is improved. The largest effect is observed at 4 g L^{-1} of NE (optimal concentration), which gives R_{ct} value equal to 164.90 Ω cm^2. This behavior can be explained by the adsorption process, i.e., NE molecules adsorb on the surface of the electrode forming a protective layer that isolates the electrode from the corrosive environment and prevents the transfer process (mass and charge transfer) (Sedik et al., 2020; Mourya et al., 2014). Furthermore, we can see that when the inhibitor concentration increases, the C_{dl} values drop. This regression might be due to a reduction in the local dielectric constant and/or a rise in the thickness of the electrical double layer, implying that the NE extract molecules work via adsorption at the metal/solution interface (de Britto Policarpi and Spinelli, 2020; Mourya et al., 2014; Fawzy et al., 2018). As can be seen from Table 2, the inhibitory effectiveness (IE) increases rapidly with inhibitor concentration and the maximum value equal to 73.31% at 4 g L^{-1} (optimal concentration) of NE. As an indication, the inhibition efficiency calculated from the electrochemical impedance findings confirms those obtained from polarization curves and mass loss methods.

3.5. Electrochemical potential noise

Electrochemical potential noise (EPN) is a non-destructive technique that consists in measuring the corrosion potential of the electrode without imposing an external source. This technique is widely used to study the corrosion of metals and considered as a complementary technique to electrochemical impedance (Ramezanzadeh et al., 2014). The EPN is performed to evaluate the inhibitory effectiveness of NE against corrosion of mild steel specimens immersed in sulfuric acid medium.

The electrochemical potential noise measurements are composed of a DC trend and potential fluctuations. For analyzing the EPN, the DC trend must be eliminated. Several methods have been employed to remove the DC trend including linear trend removal, moving average removal, Wavelet Analysis and polynomial fitting etc. Polynomial fitting has been proposed for DC trend removal, it is a powerful method to remove just the drift part without impacting the meaningful information. After removing the DC trend, the EPN data were analyzed in the frequency domain to generate the power spectral density (PSD) and by statistical analysis to obtain the standard deviation (STD), Skewness (SK) and Kurtosis (KU).

The STD describes the intensity of a signal and is assimilated to the instantaneous power of the electrochemical noise. It is determined by the following formula (Shahidi et al., 2012; Bahrami et al., 2014).

$$STD = \sqrt{\frac{\sum_{i=1}^{N}\left(E_i'(t) - \bar{E'}\right)^2}{N}} \tag{11}$$

The skewness coefficient measures the asymmetry of a statistical random variable. When the distribution is symmetrical, the SK equals zero (Mansfeld et al., 2001; Cottis et al., 2001):

$$SK = \frac{\frac{1}{N}\sum_{i=1}^{N}\left(E_i'(t) - E^{-\prime}\right)^3}{STD^3} \tag{12}$$

The kurtosis coefficient (KU) measures the distribution shape of a statistical random variable. When the distribution is normal, the KU equals zero (Maizia et al., 2018):

$$KU = \frac{\frac{1}{N}\sum_{i=1}^{N}\left(E_i'(t) - E^{-\prime}\right)^4}{STD^4} - 3 \tag{13}$$

3.5.1. Direct analysis of electrochemical potential noise (EPN)

Fig. 6 shows the electrochemical potential noise with time in the presence and absence of NE in 0.5 mol/L H_2SO_4 medium.

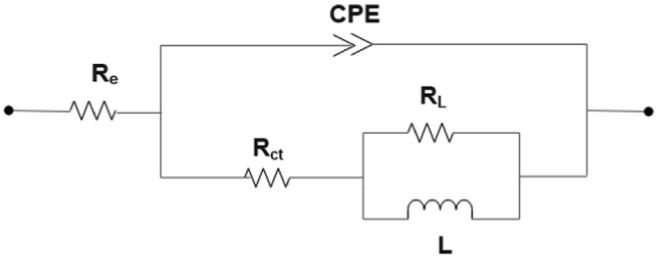

Fig. 5 Electrical equivalent circuit diagram used to fit the EIS data of mild steel electrode in 0.5 M H_2SO_4 solution with and without NE.

Table 2 EIS parameters for the corrosion of mild steel immersed in 0.5 M H_2SO_4 medium without and with different concentrations of NE.

Concentration (g L^{-1})	R_e (Ohm cm^2)	$Q \times 10^{-5}$ (S^n Ohm^{-1} cm^{-2})	n	R_{ct} (Ohm cm^2)	$C_{dl} \times 10^{-4}$ (mF cm^{-2})	IE (%)	χ^2 (10^{-4})
0	9.70	6.00	0.85	44.01	70.39	–	7.10
0.4	9.77	5.93	0.84	70.54	12.18	37.61	8.00
0.8	9.76	7.06	0.81	124.6	0.91	64.68	9.43
1.2	9.89	5.00	0.82	131.1	2.11	66.43	7.47
2.0	9.63	6.77	0.79	157.3	1.09.	72.02	7.00
4.0	9.70	6.70	0.82	164.9	0.46	73.31	5.83
6.0	9.70	5.36	0.80	137.8	0.58	68.06	8.12

It can be clearly seen that adding NE inhibitor has reduced the amplitude (intensity) of the potential fluctuations. This indicates that the electrochemical events (electrochemical reactions and mass transfer phenomena…) on the metal surface are hindered by the adsorption of the inhibitor NE on the electrode surface.

From Table 3, it appears that the amplitude of the electrochemical potential noise (ΔE) is higher in the absence of the inhibitor and at lower concentrations of NE ($C \leq 0.8$ g L^{-1}) compared to the higher concentrations of NE ($C > 0.8$ g L^{-1}), i.e., the increasing of NE concentrations decreases the amplitude of the EPN. The lowest amplitude was obtained at $C = 4$ g L^{-1}. Furthermore, the ΔE value without NE inhibitor is about 20 times larger with the presence of NE. These observations reveal that this inhibitor is very effective against corrosion.

3.5.2. Power spectral density analysis (PSD)

PSD is one of the most popular methods for the analysis of electrochemical noise in the frequency domain (Zhang et al.,

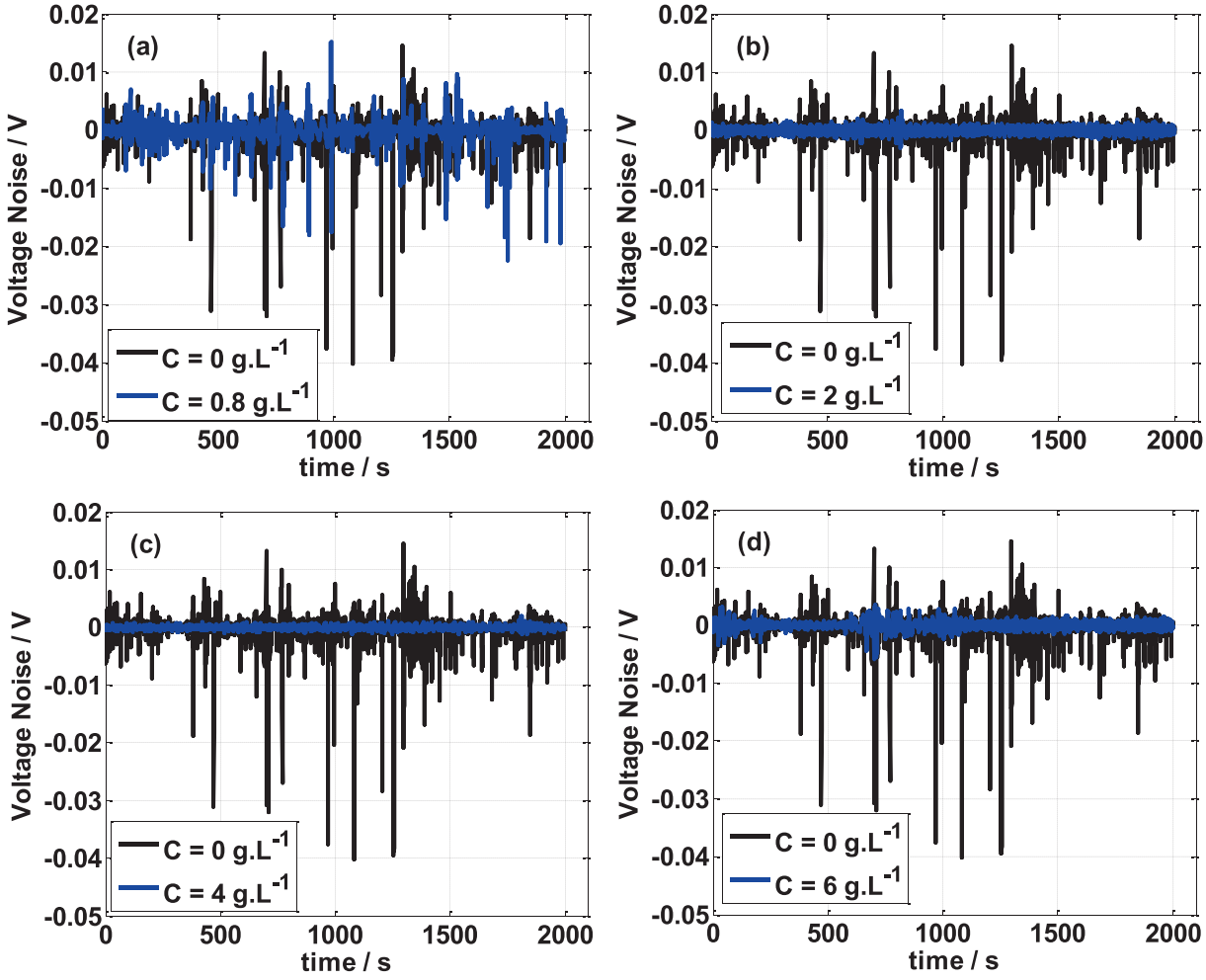

Fig. 6 Voltage noise vs time at various concentrations of NE and T = 25 °C.

Table 3 Electrochemical potential noise amplitude with and without of NE in 0.5 M H_2SO_4 at T = 25 °C.

C/ g.L^{-1}	0	0.8	2	4	6
Amplitude (ΔE)/ V	0.0546	0.0323	0.0064	0.0029	0.0094

2018). Fig. 7 shows the PSD spectra as a function of frequency without and with varying amounts of NE at T = 25 °C. All power spectral densities (PSD) highlight the same shape, only the amplitude of PDS (ordinate value) which change, and PSD is inversely proportional to the frequency ($PSD = 1/f^{\alpha}$). Furthermore, it is observed that the addition of the NE inhibitor led to the decrease in the amplitude of the spectra and the lowest magnitude of the PSD plot was observed at C = 4 g L^{-1} (optimal concentration). This implies that mild steel is more resistant to corrosion in sulfuric acid solution in presence of NE inhibitor. We can conclude that, the addition of an effective concentration of NE successfully reduces the corrosion rate of steel by building a protective layer that covers the majority of the corrosion active sites (Mehdipour et al., 2015).

3.5.3. Statistical analysis

STD is one of the simplest parameters for measuring the amplitude of the electrochemical noise fluctuations (Shi et al., 2006). Fig. 8 compares the standard deviation of mild steel specimens exposed to different concentrations of NE (0.8, 2, 4, and 6 g L^{-1}) and without NE in 0.5 mol/L H_2SO_4 medium. It is clear that, the STD amplitude is more pronounced and unstable without inhibitor and for lower values of NE concentrations (C ≤ 0.8 g L^{-1}). The instability of STD values is due to the corrosion reactions (hydrogen evolution and/or dissolution of metal) of mild steel samples. On the other hand, at C > 0.8 g L^{-1} of NE (presence of the inhibitor), it is found that the standard deviation is more stable and invariant with time. For comparison, the value of standard deviation in the absence of NE is twenty times higher than in the presence of the NE inhibitor. The lower STD value indicates a better anticorrosive efficiency of NE. Moreover, the largest effect was observed at C = 4 g L^{-1} of NE which gives a STD value equal to 0.00038 V. The adsorption process of NE can explain this behavior, i.e., the molecules of the NE inhibitor adsorb on the electrode surface forming an insulating layer that separates the electrode surface from the corrosive solution.

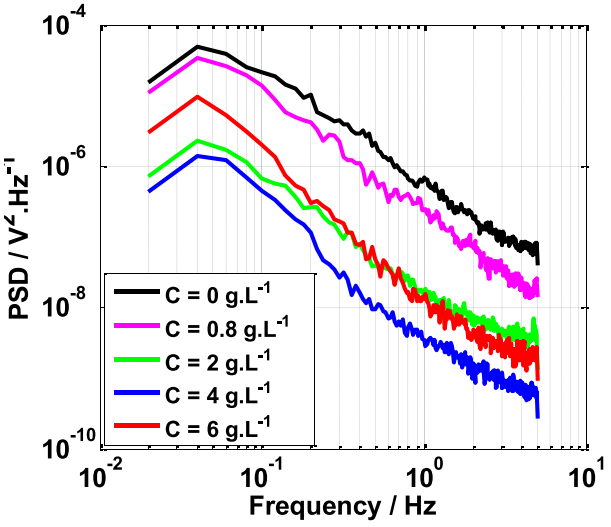

Fig. 7 Power Spectral Density vs Frequency at various concentrations of NE and T = 25 °C.

Fig. 9 shows a comparison of the Skewness of mild steel specimens exposed to different concentrations of NE with the Skewness values obtained without addition of NE in 0.5 mol/L H_2SO_4 medium. It can be seen that the SK in the absence of NE and at very low concentrations of NE (C < 0.8 g L^{-1}) reveals a notable variation and varies with time. For C = 0.8 g L^{-1}, SK varies between −4 to 2 and without NE, SK is more fluctuating; its magnitude varies between −9 to 2. The large values of SK and its variations with time are due to the dissolution of the working electrode affected by the aggressive ions of the sulfuric acid. On the other hand, it is clear that in the presence of the inhibitor NE i.e., at C > 0.8 g L^{-1}; SK is most stable with time and varies around zero. This confirms the protection of the working electrode by the NE inhibitor.

Fig. 10 compares the Kurtosis of mild steel specimens exposed to different concentrations of NE and without NE in 0.5 mol/L H_2SO_4 medium. Fig. 10**a** shows that Kurtosis without NE inhibitor is very intermittent and oscillates; most of the time is positive and varies from 0 to 80. However, in the presence of the NE inhibitor (C > 0.8 g L^{-1}), the KU is stable and close to zero. This confirms the effectiveness of this inhibitor to protect mild steel from corrosion. From the statistical analysis, we can conclude that in the presence of the NE inhibitor, the distribution is normal (Gaussian) because SK and KU are equal to zero. Conversely, in the absence of the NE inhibitor the distribution is non-Gaussian.

The statistical analysis of standard deviation, skewness, and kurtosis reveals improved electrochemical stability and anticorrosive efficiency at concentrations higher than 0.8 g L^{-1}, with the most significant effect observed at 4 g L^{-1}. The NE inhibitor adsorbs on the electrode surface, forming a protective layer and resulting in a normal distribution of electrochemical noise parameters, confirming its role in mitigating corrosion.

3.6. Adsorption isotherms

The effectiveness of a corrosion inhibitor strongly depends on its adsorption ability on the electrode surface. Several adsorption isotherms, including Langmuir, Temkin, and Frumkin, can be used to investigate the interactions between the inhibitor and the steel surface (Khaled, 2008). The best fitting of the experimental data (R^2 = 0.99) obtained from EIS analysis was acquired with Langmuir isotherm as shown in Fig. 11. Langmuir adsorption isotherm is expressed with Eq. (14) (Benmahammed et al., 2020):

$$\frac{C}{\theta} = \frac{1}{K_{ads}} + C \tag{14}$$

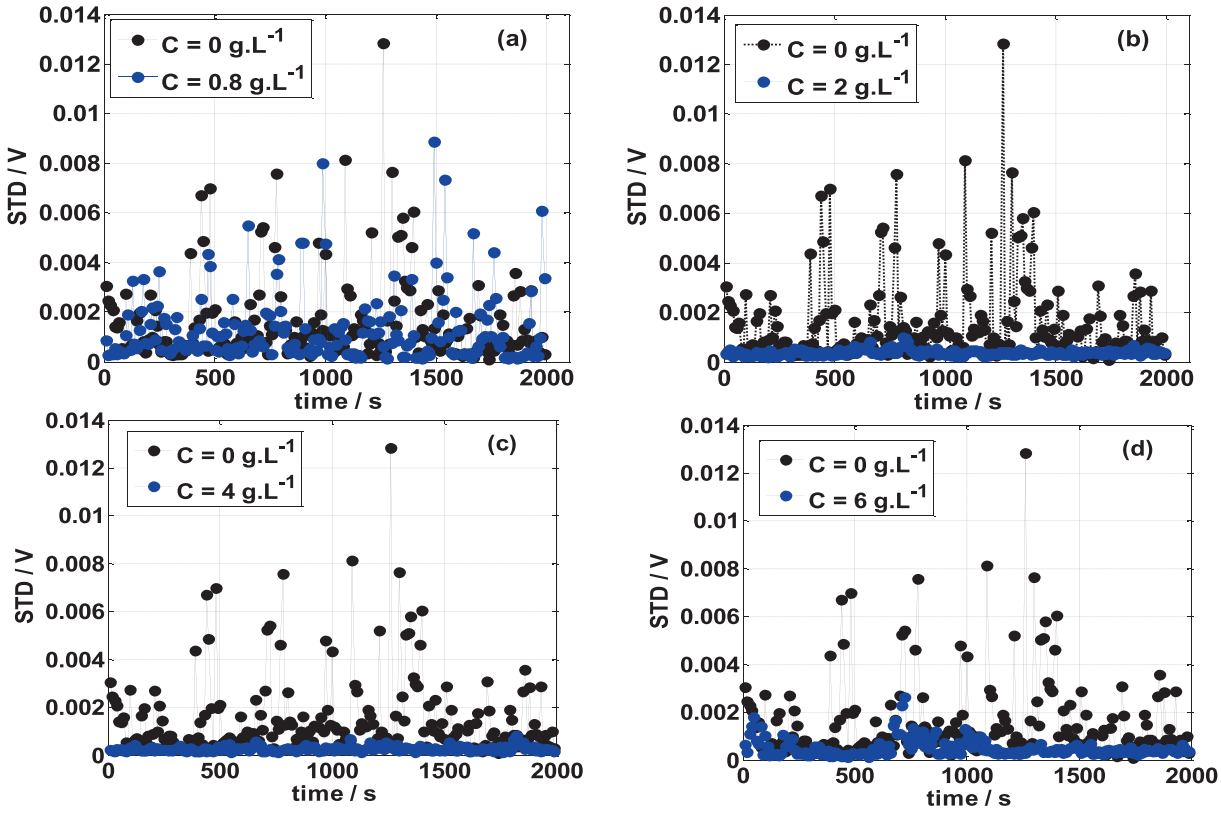

Fig. 8 Standard deviation vs time at various concentrations of NE and T = 25 °C.

Where (C) is the NE concentration; (K_{ads}) represent the adsorption constant, (θ) represent the surface coverage.

Gibbs free energy (ΔG_{ads}) is another parameter that may be calculated from the adsorption isotherm. The equation (15) may be used to compute the value of ΔG_{ads} (Benmahammed et al., 2020):

$$\Delta G_{ads} = -RT\ln(55.5K_{ads}) \quad (15)$$

Where, (R) is the universal gas constant, T and K_{ads} are temperature in kelvin and adsorption constant, respectively.

According to the literature, the negative value of the standard Gibbs energy implies that the inhibitor is spontaneously adsorbed on the steel surface. When ΔG_{ads} is less than 20 kJ.mol^{-1}, it implies physisorption, but when it is greater than 40 kJ.mol^{-1}, it indicates chemisorption. However, if the value of ΔG_{ads} is between 20 and 40 kJ.mol^{-1}, it is assumed that the adsorption includes both physisorption and chemisorption processes (Keramatinia et al., 2019). The value of ΔG_{ads} in this investigation is between 20 and 40 kJ.mol^{-1} ($\Delta G_{ads} = -26.69 kJ.mol^{-1}$), which corresponds to both physisorption and chemisorption processes.

3.7. Effect of temperature

Temperature is a critical element to investigate the inhibitory efficiency of this inhibitor at high temperatures. For this purpose, the intensity-potential tests were carried out in the absence and presence of the optimum concentration of NE (C = 4 g L^{-1}) at varied temperatures. The Arrhenius equation describes the relationship between corrosion rate (current density) and temperature (de Britto Policarpi and Spinelli, 2020):

$$i_{corr} = A\exp(\frac{-E_a}{RT}) \quad (16)$$

where, R = 8.314 Jmol^{-1}K^{-1} is the gas constant, i_{corr} is the corrosion current density, A is the frequency factor, E_a is the activation energy and T is the temperature. In the absence and presence of the optimal concentration of NE, Fig. 12 depicts the Arrhenius curves (ln (i_{corr}) vs. 1/T). In both, with and without NE inhibitor, the corrosion rate increases as the temperature rises, but the rate is greater in the absence of the inhibitor. This shows that the NE inhibitor is still effective at higher temperatures and may preserve the steel against corrosion. The activation energy values (E_a) were calculated from the Arrhenius curves using equation (14) (Hassanien and Akl, 2018, 2016a, 2016b), which are 24.87 and 49.32 kJ mol^{-1} without and with NE, respectively. We can notice that when NE is present, E_a is about 2 times greater than when it is absent, implying that the energy barrier for the occurrence of the oxidation process is raised and the corrosion kinetics is delayed (de Britto Policarpi and Spinelli, 2020).

3.8. Surface studies

3.8.1. Contact angle measurements

This technique provides crucial information about the surface state, such as electrode surface modification and surface hydrophilic or hydrophobicity (Sedik et al., 2020). Fig. 13 depicts the contact angle of steel electrodes after 4 h of exposure in 0.5 mol/L H_2SO_4 medium without and with varied amounts of NE. Results from this figure shows that the contact angle value of steel rises with the addition of NE inhibitor concentration, i.e., the contact angle rises from around 33 to 85°

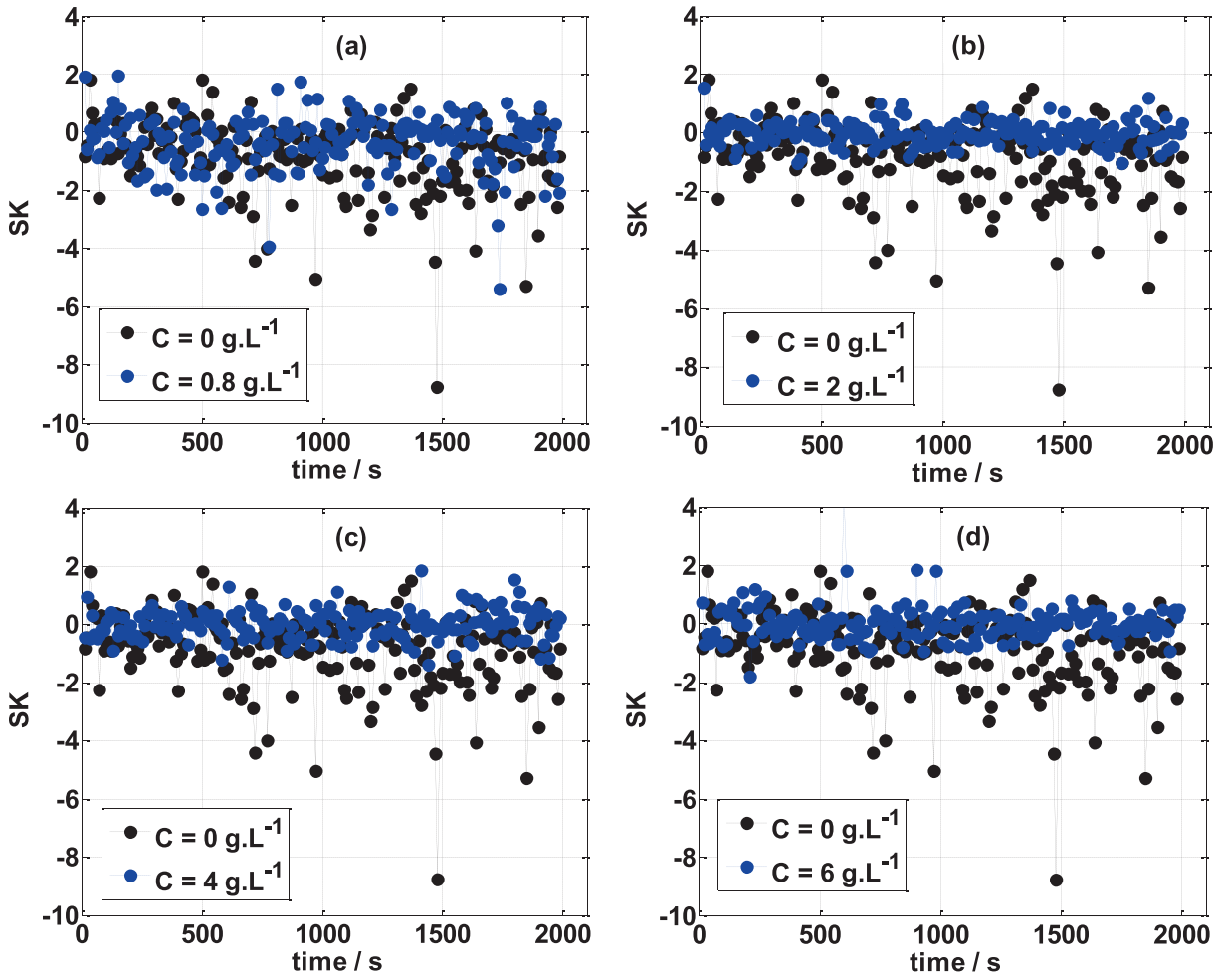

Fig. 9 Skewness vs time at various concentrations of NE and T = 25 °C.

with the addition of NE in the solution from 0 to 4 g L^{-1}. Furthermore, the largest value of the contact angle was observed at C = 4 g L^{-1} of NE which corresponds to the optimum concentration. The increase in the contact angle value, could be explained by the development of an organic layer on the steel surface, having a hydrophobic character, which led to the protection of the steel electrode against corrosion (Sedik et al., 2020; Yeganeh et al., 2020).

3.8.2. XRD analysis

The XRD study was employed to examine the steel surface after exposure in 0.5 mol/L H_2SO_4 medium without and with NE inhibitor and the XRD patterns are shown in Fig. 14. According to Fig. 14**a**, the XRD pattern of the steel sample without inhibitor shows several peaks associated to corrosion products and iron metal such as FeOOH at 2θ = 34.98°, Fe_3O_4 at 2θ = 18.16°,Fe_2O_3 at 2θ = 37,87°, 48.9° and Fe metal at 2θ = 44.92°, 64.78° (Loganayagi et al., 2014; Chung et al., 2018). On the other hand, the sample submerged in the H_2SO_4 solution containing 4 g L^{-1} of NE (Fig. 14**b**), illustrates only the peak related to the Fe metal at 2θ = 44.92, 64.78° i.e., the iron oxide peaks (corrosion products) have disappeared. These results confirm the effective effect of the inhibitor in protecting the sample from corrosion by an adsorption action on the steel surface.

3.8.3. Optical microscopy characterization

Fig. 15 shows the optical images of mild steel surface before immersion (Fig. 15**a**), exposed during 3 h in 4 g L^{-1} of NE (Fig. 15**b**) and without NE (Fig. 15**c**). The image of the steel surface before immersion (Fig. 15**a**) shows a bright and smooth surface. The picture of the mild steel surface after immersion in the H_2SO_4 solution containing 4 g L^{-1} of NE (Fig. 15**b**) is similar to that before immersion (no significant difference) and without any apparent traces of corrosion products (XRD analysis shows only iron peaks). However, the image of the mild steel surface after immersion in absence of NE inhibitor (Fig. 15**c**), is highly damaged with appearance of several black spots on the surface which corresponds to the corrosion products. The black spots indicate that the metal underwent severe corrosion by the aggressive medium. We can conclude that the NE can effectively protect X38 steel.

3.9. Quantum chemical calculations

In the last two decades, quantum chemical calculations have been one of the most popular methods for studying the reactivity of an inhibitor and its ability to inhibit metal corrosion. To obtain additional insights on the reactivity of NE's components and potential adsorption sites of Histamine, serotonin, quercetin, kaempferol, some quantum chemical parameters

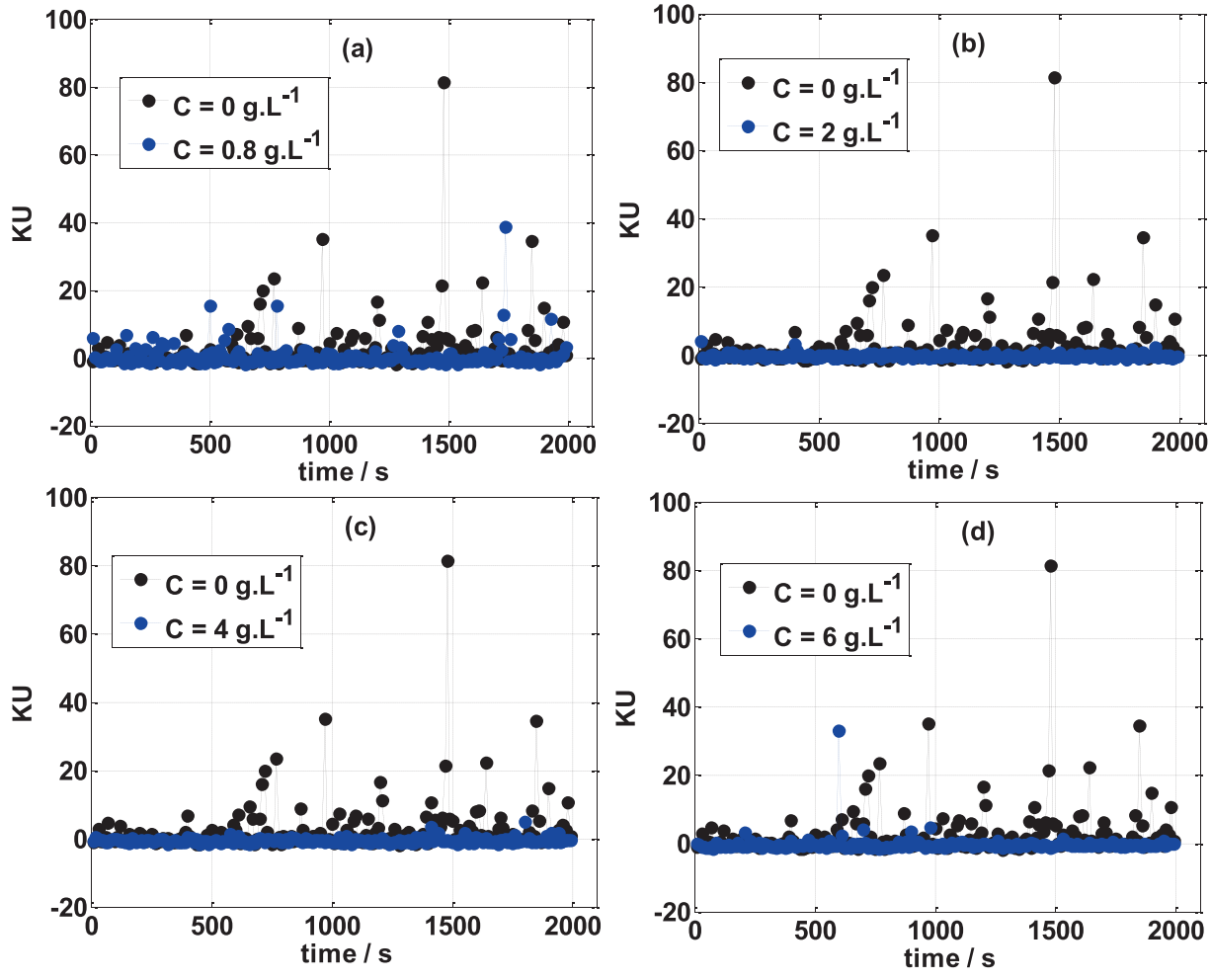

Fig. 10 Kurtosis vs time at various concentrations of NE and T = 25 °C.

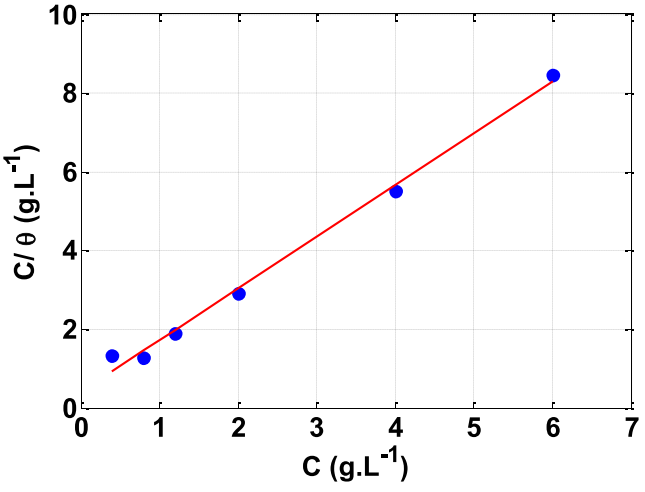

Fig. 11 Langmuir adsorption isotherm of NE inhibitor in 0.5 M H_2SO_4 at 25 °C.

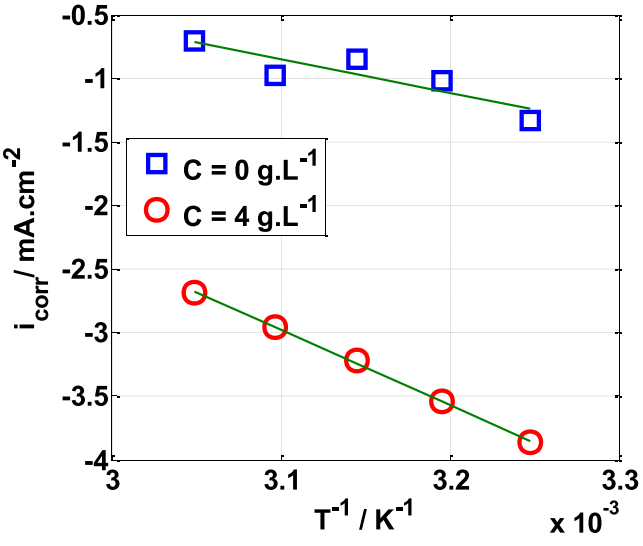

Fig. 12 Arrhenius plots of ln (i_{corr}) vs 1/T for mild steel in 0.5 M H_2SO_4 solution without and with NE.

were generated after complete geometry optimization of these components by DFT method in water phase. In this regard, the optimized structure, electrostatic potential map (ESP) and Mullikan charge are illustrated in Fig. 16, frontier mole-

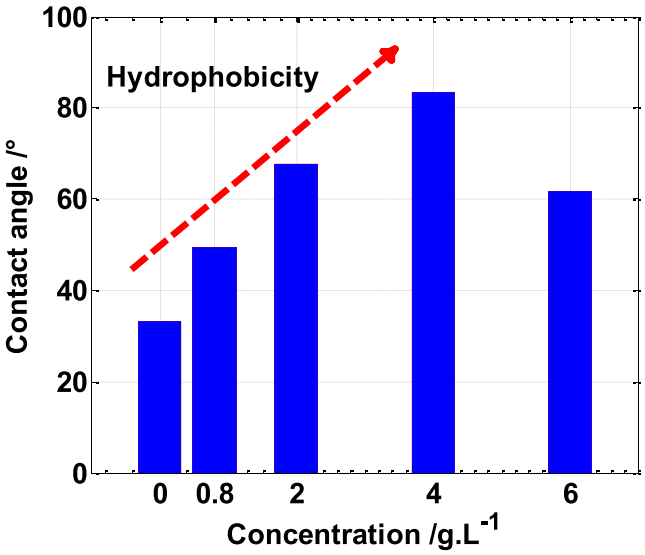

Fig. 13 Contact angle measurements of the mild steel after four hours of immersion in 0.5 M H_2SO_4 solution, without and with different concentrations of NE.

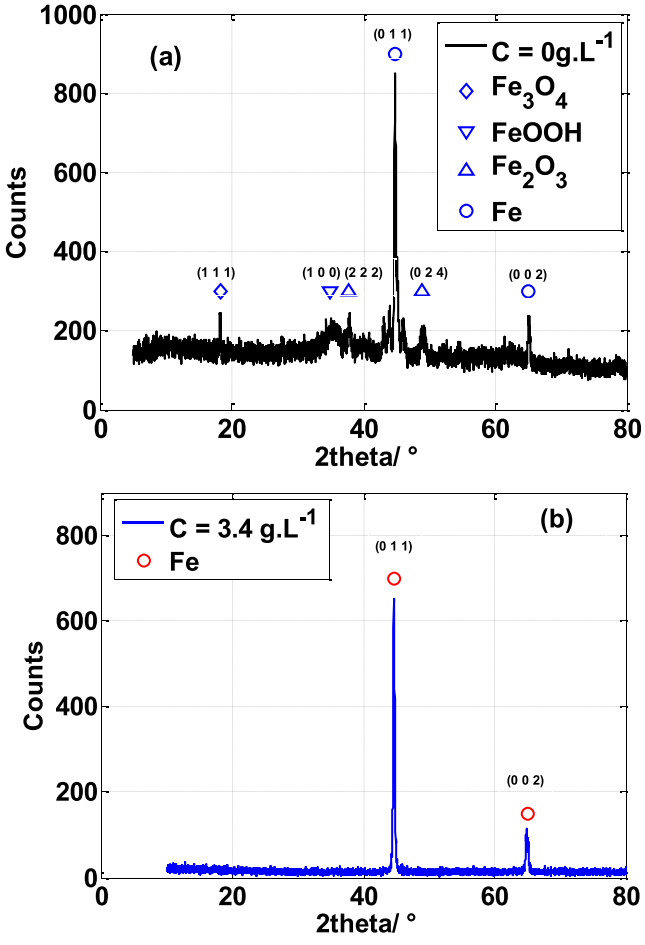

Fig. 14 X-ray diffraction patterns of mild steel exposed in 0.5 M H_2SO_4 for 24 h: **(a)** without, and **(b)** with NE inhibitor at temperature 25 °C.

cule orbital density distributions namely, HOMO and LUMO are shown in Table 4, while numerous quantum chemical parameters related to the reactivity of basic components of NE are recorded in Table 5.

The Molecular electrostatic potential (MEP) is a very useful parameter that offers information about the reactive sites (electrophilic attacks and nucleophilic reactions) (Abdallah et al., 2021). Fig. 16 illustrates the values of the electrostatic potential of the basic components of NE inhibitor (Histamine, serotonin, quercetin, kaempferol) which are represented by different colors. This figure shows that the negative electrostatic potential is represented by red to yellow color, where high electron density (nucleophilic reaction) exists, while the positive regions are represented by blue color (electrophilic reaction). In addition, the green and white colors correspond to the zero potential area. As it is observed, the negatively charged regions are located in heteroatoms and benzene chains, such as O, N atoms and around some carbon atoms on their side or O-heterocyclic and N-heterocyclic rings. Indeed, the electron-rich sites (negative sites) are the ideal sites for the adsorption of NE compounds on the metal surface (Panicker et al., 2015). On the other hand, the sites with positively charged areas (poor in electrons) are located on some carbon and nitrogen atoms.

Fig. 16 represents the Mulliken charges distribution of the basic components of NE (Histamine, serotonin, quercetin and kaempferol). According to Fig. 16, all heteroatoms (N and O atoms) and some carbon atoms (benzene rings and double bonds) have negative charges with high electron density; these atoms are the potential active sites of adsorption. Therefore, NE inhibitor can be adsorbed on the steel surface using these active centers, then decreasing the corrosion rate (Chafiq et al., 2020; Özcan et al., 2004). Conversely, the positive charges are located in the remaining carbon atoms of the basic components of NE; these atoms are active sites accepting electrons from the steel orbitals to form bonds of *retro*-donation.

The HOMO and LUMO are very crucial parameters for predicting a molecule's adsorption centers, particularly donor and acceptor sites (El Bakri et al., 2019). Optimized structures and frontier molecular orbitals of the basic components of NE inhibitor are shown in Table 4. The HOMO indicates that NE has a good ability to give electrons to the vacant *d*-orbital of steel surface, while the LUMO implies that NE has an affinity for accepting electrons from the *d*-orbitals of the steel electrode (Abdallah et al., 2021). It is evident from Table 4 that the HOMO and LUMO electronic densities are distributed around the entire surface of the basic components of NE. Indeed, the NE inhibitor can potentially accept and donate electrons at the same time.

The quantum chemical parameters are listed in Table 5. The E_{HOMO} value indicates better ability of NE to donate electrons to the steel electrode, while a lower E_{LUMO} value indicates better ability of an inhibitor to accept electrons from the steel surface. The reported results in Table 5 illustrate that the order of E_{HOMO} in the aqueous phase is Serotonin > Quercetin > Kaempferol > Histamine, indicating that Serotonin and Quercetin have a higher ability to donate electrons to the surface of the mild steel. The order of E_{LUMO} is Quercetin < Kaempferol < Serotonin < Histamine, indicat-

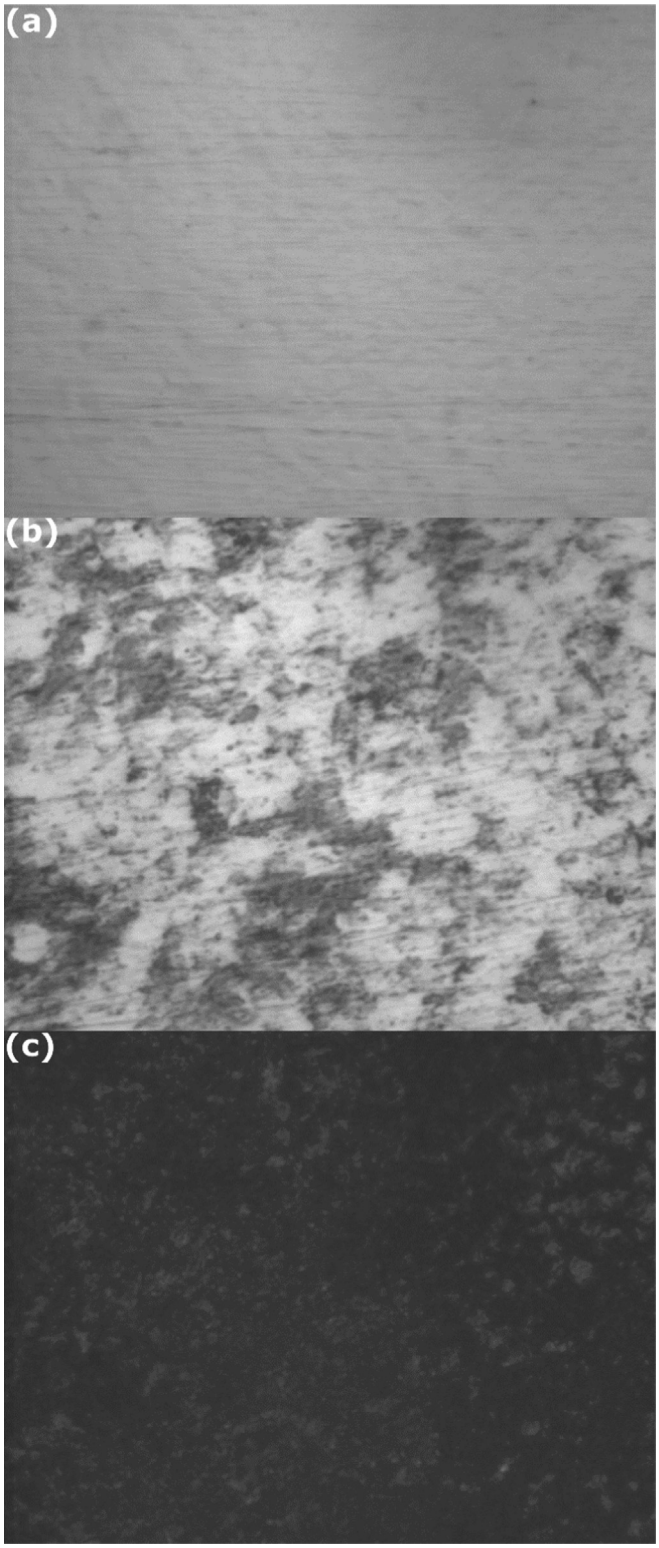

Fig. 15 Optical images of mild steel samples at mag. x40:**(a)** before immersion; **(b)** after three hours of immersion in 0.5 M H_2SO_4 with 4 g $L^{-1}$of NE; **(c)** after three hours of immersion in 0.5 M H_2SO_4 without NE.

ing that Quercetin and Kaempferol have a stronger chance of accepting electrons from the metal.

The energy gap (ΔE) is a performance indicator for predicting the reactivity of NE components; a low value of ΔE is generally linked with strong chemical reactivity and hence higher inhibition efficiency (Abdallah et al., 2021). As shown in Table 5, Quercetin and Kaempferol showed higher reactivity.

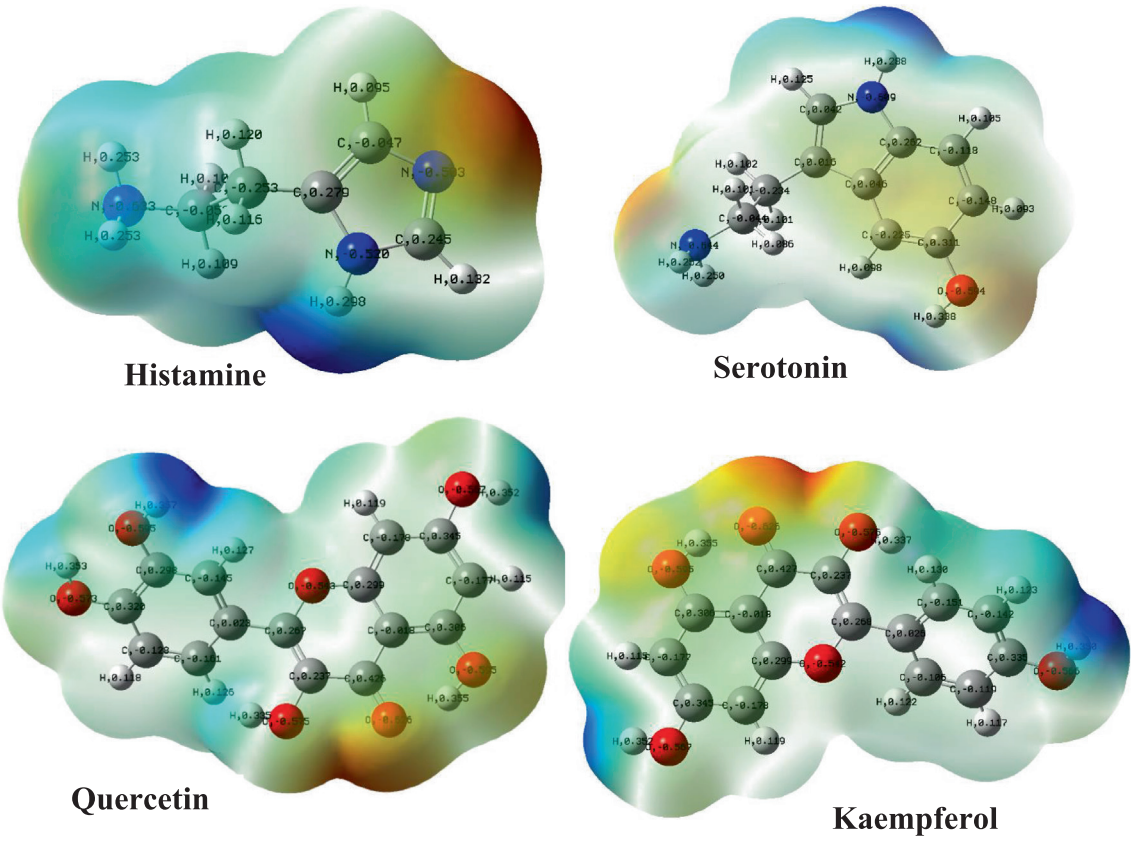

Fig. 16 The electrostatic potential maps and Mulliken atomic charges of the four basic components of NE.

Global softness and hardness play a prominent role in estimating the reactivity trend of a molecule. A low value of hardness (η) and a high value of softness (σ) are associated with high inhibition efficiency. As presented in Table 5, Quercetin and Kaempferol have low hardness (η) values and high softness (σ) values implying that they have potentially better chemical reactivity towards the metal surface.

The fraction of electron transferred (ΔN) value measures the capacity of the inhibitor molecule to donate its electrons to the steel electrode if ΔN is greater than zero and vice versa (Abdallah et al., 2021; El Bakri et al., 2019). The positive value of ΔN (Table 5) indicates that the four basic components of NE have a strong ability to donate electrons to the steel electrode and the trend increases as follows: Quercetin > Kaempferol > Serotonin > Histamine. In summary, quantum chemical parameters demonstrate that nettle extract's components have good inhibitory properties against corrosion of steel samples.

3.10. DFTB modeling

3.10.1. Optimized adsorption geometries

Quantum chemical calculations and its related global reactivity descriptors have been used for many years to discuss and interpret the corrosion inhibition performance of corrosion inhibitors. Like in our previous section, quantum chemical calculations can be useful for investigating the reactivity of compounds such as potential adsorption sites and preferred optimized geometry, however, the molecule's electronic behavior can be totally different when it approaches another chemical species such as a metal surface (Kokalj, 2010). Therefore, it would be useful to study the adsorption characteristics of compounds when interacting with the metal surface (Kokalj, 2022). To this end, the adsorption of Quercetin, Kaempferol, Serotonin, and Histamine on the Fe(1 1 0) surface has been modelled and investigated using DFTB simulation. Fig. 17 and Fig. 18 represent the most stable adsorption geometries of Quercetin, Kaempferol, Serotonin, and Histamine molecules on Fe(1 1 0) surface in their parallel and perpendicular initial configurations, respectively. By inspecting Fig. 17, one can notice that all molecules, except HIST, kept the initial adsorption configuration, and formed bonds with Fe atoms. The SERO molecule forms two bonds with Fe atoms with 2.21 Å and 2.31 Å length distances. QUER and KAEM molecules, which have similar molecular structures form several bonds with the Fe atoms with length distances between 1.98 Å and 2.33 Å. In the case of QUER and KAEM molecules, both carbon and oxygen atoms are bonding with Fe atoms while only carbon atoms are involved in interactions between SERO and Fe(1 1 0) surface. The HIST molecule does not form any bond with the metal surface and its nitrogen atoms are around 3 Å from the upper iron surface, which suggest that it is probably interacting with Fe(1 1 0) surface through van der Walls interactions (Kumar et al., 2022; Kumar et al., 2020b).

Moving to the perpendicular initial geometries, we can observe that after DFTB optimization, only QUER and KAEM molecules are able to bond with Fe atoms mainly through oxygen atoms. The QUER molecule form three bonds between oxygen and Fe atoms with length distances of 2.03 Å, 1.95 Å, and 1.86 Å. The KAEM molecule, on the other hand,

Table 4 The frontier molecular orbitals (HOMO and LUMO) and the optimized structures of the four basic components of NE.

Constituents	Optimized structures	Frontier molecular electron distribution	
		HOMO	**LUMO**
Histamine	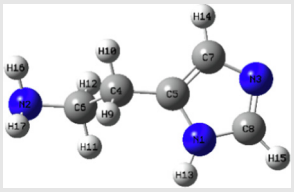	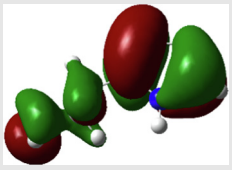	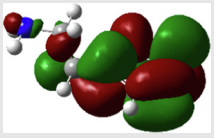
Serotonin	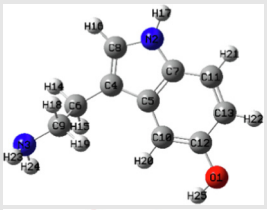	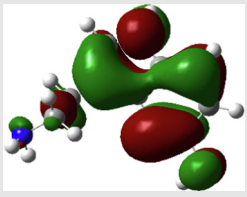	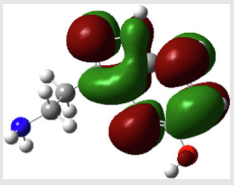
Kaempferol	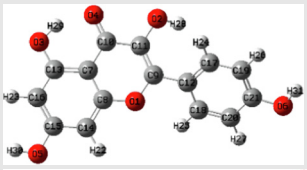	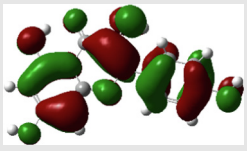	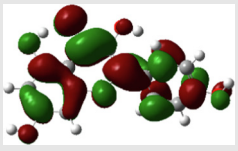
Quercetin	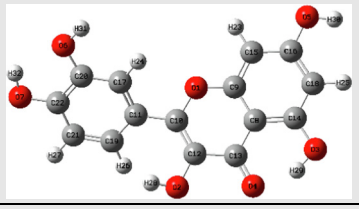	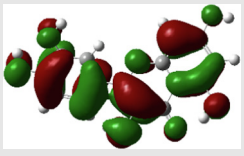	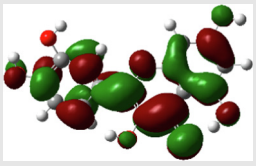

Table 5 The Quantum chemical parameters of the four basic components of NE.

Parameters	Constituent			
	Histamine	Serotonin	Kaempferol	Quercetin
E_{tot} (A.U)	−360.2200	−573.0400	−1028.9900	−1104.2100
$E_{HOMO\ (eV)}$	−0.21610	−0.19550	−0.210970	−0.20870
$E_{LUMO\ (eV)}$	0.02979	−0.01049	−0.06580	−0.06621
$\Delta E_{\ (eV)}$	0.24590	0.18500	0.14520	0.14250
$A_{\ (eV)}$	−0.02979	0.01049	0.06580	0.06621
$I_{\ (eV)}$	0.21610	0.19550	0.210970	0.20870
$\eta_{(eV)}$	0.1229	0.0925	0.0726	0.0712
σ^{-1}_{eV}	8.1337	10.8102	13.7770	14.0361
$\chi_{\ (eV)}$	0.0932	0.1030	0.1384	0.1375
μ (Debye)	4.7641	1.5024	6.3954	7.8758
ΔN	19.2234	25.4959	32.2492	32.8623

forms two bonds between a single oxygen atom and Fe atom, with bond distances of 2 Å. SERO and HIST molecules are probably interacting via physical interactions. The length distances of the formed bonds can be compared with the sum of the covalent radii of each pair of atoms. The sums of the covalent radii for Fe-C and Fe-O are $r_C + r_{Fe} = 2.08$ Å and $r_O + r_{Fe} = 1.98$ Å, respectively (Cordero et al., 2008). Therefore, it can be seeing that all formed bonds between C/O of NE's molecules and Fe atoms are within the sums of covalent radii, suggesting that interactions are most probably chemical in nature (Kumar et al., 2022; Kumar et al., 2020b).

The adsorption binding energy of SERO, QUER, KAEM, and HIST parallel adsorption systems are −1.04, −2.35, −1.98, and −0.63 eV, respectively. For perpendicular adsorp-

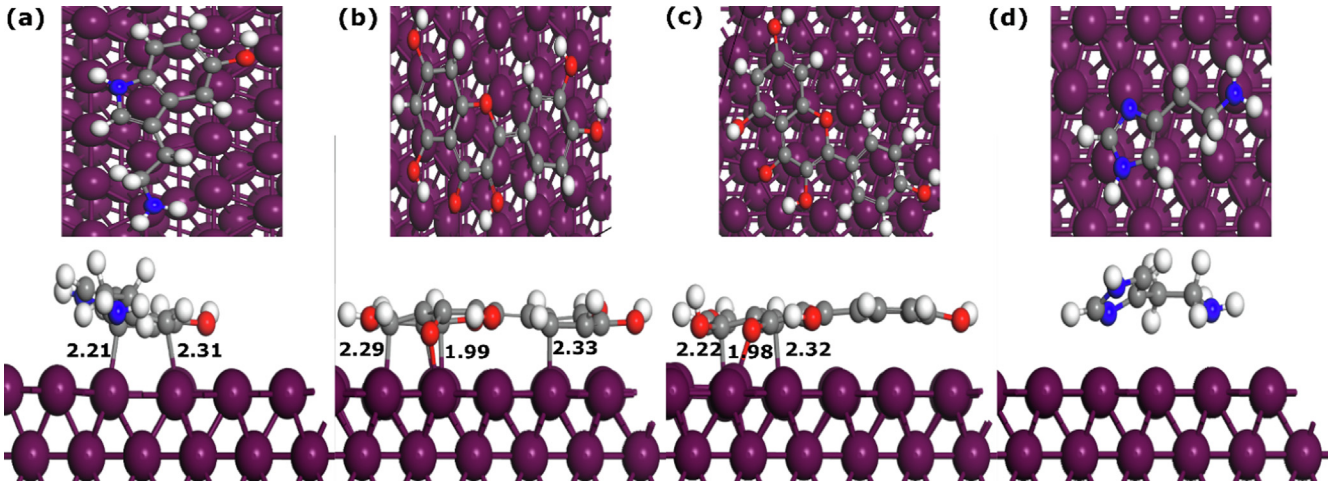

Fig. 17 The DFTB optimized parallel adsorption geometries of NE components adsorbed on Fe(1 1 0) surface. (a)-(d) are SERO, QUER, KAEM, and HIST, respectively. Bond distances are in Å.

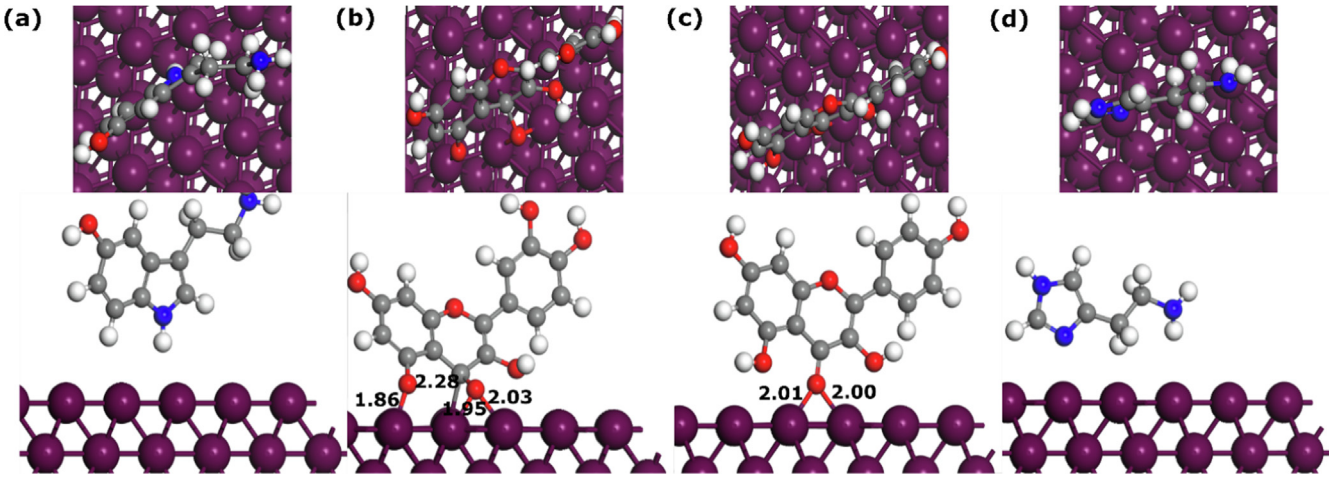

Fig. 18 The DFTB optimized perpendicular adsorption geometries of NE components adsorbed on Fe(1 1 0) surface. (a)-(d) are SERO, QUER, KAEM, and HIST, respectively. Bond distances are in Å.

tion configurations, the adsorption binding energies are −0.54, −1.66, −0.89, and −0.59 eV for SERO, QUER, KAEM, and HIST, respectively. The molecules bonding with the metal surface have the most negative binding energies, suggesting that are energetically more stable (Kokalj et al., 2020; Dlouhy and Kokalj, 2022). The interactions between NE's components and Fe(1 1 0) surface might involve contribution of physical interactions in addition to chemical bonding. Further investigation of the nature of interactions between NE's components and Fe(1 1 0) surface can be performed by analyzing the projected density of states of molecules in their isolated and adsorbed states.

3.10.2. Projected density of states

Projected density of states can provide deep insights into the bonding mechanism, and particularly the potential charge transfer between investigated molecules and the metal surface (Chafiq et al., 2022; Thomas et al., 2014). Fig. 19 represents the projected electronic density of states (PDOS) on NE's molecules in their isolated (Fig. 19(a)-(d)) optimized parallel geometries (Fig. 19(a')-(d')), and optimized perpendicular geometries (Fig. 19(a")-(d")). Based on several previous reports, the Fe-3d valence states lie in the −5/5 energy range, thus the −5/5 energy range is considered for all molecules (Kumar et al., 2020a). From Fig. 19(a)-(d), one can notice that molecular states, including those lying within the energy range of the Fe-3d-band are very sharp and intense. In the parallel adsorption geometries (Fig. 19(a')-(d')), one can notice that most of peaks that lie at the position of iron *d*-band decrease and show significant broadening, suggesting a high hybridization of Fe-3d and molecules-2p orbitals (Kumar et al., 2020b). The chemical states of the HIST molecule show no significant changes attributed to the physical interactions with the Fe(1 1 0) surface. Concerning the perpendicular adsorption geometries, it can be noticed that changes in the chemical sates are significant for KAEM and QUER molecules, however, no changes are observed for the other molecules, i.e., SERO and HIST because of their physical interactions with Fe(1 1 0) surface.

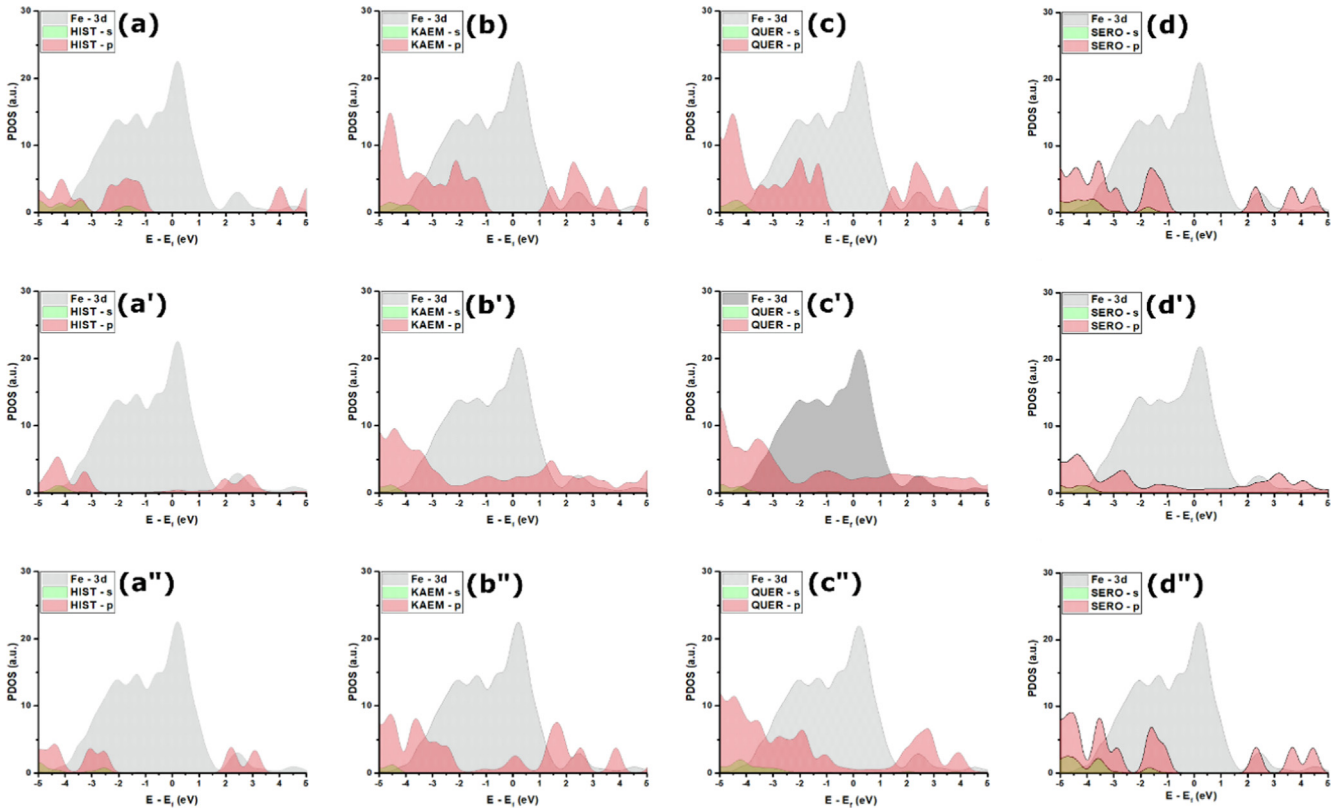

Fig. 19 Projected density of states of SERO, QUER, KAEM, and HIST at their (a)-(d) isolated, (a')-(d') parallel adsorption on Fe(1 1 0) surface, and (a")-(d") perpendicular adsorption on Fe(1 1 0) surface.

The strong hybridization that occurred between Fe-3d and p orbitals of bonding NE's molecules suggests that interactions are based on charge transfer between molecules active sites and vacant d-orbitals or iron atoms (Kumar et al., 2020a).

4. Conclusion

In this study, the corrosion inhibition efficiency of nettle extract (NE) for mild steel in 0.5 mol/L H_2SO_4 was investigated. Our findings indicated that NE's inhibition performance improved with increasing concentration, reaching a maximum efficiency of approximately 95% at 4 g L^{-1}. NE acted as a mixed-type inhibitor, reducing anodic and cathodic current densities. Electrochemical impedance spectroscopy (EIS) results demonstrated that NE's components effectively adsorbed onto the metal surface, increasing charge transfer resistance and decreasing double layer capacitance. The adsorption of NE on mild steel followed the Langmuir adsorption model, with both physisorption and chemisorption processes taking place. Surface studies, including optical microscopy, XRD, and contact angle measurements, confirmed that NE forms a protective layer that isolates the metal from the acidic environment. Density functional theory (DFT) studies identified several reactive sites within NE's components that contribute to its corrosion inhibition performance. DFTB modeling revealed that quercetin (QUER) and kaempferol (KAEM) have the most stable adsorption geometries on the metal surface and form strong covalent bonds. Serotonin (SERO) and histamine (HIST), however, exhibited weaker binding abilities. Our results suggested that the synergistic adsorption of NE's components makes it an effective corrosion inhibitor for mild steel in sulfuric acid solutions. Based on these findings, the nettle extract can be recommended as an eco-friendly corrosion inhibitor for mild steel in acidic environments, particularly at a concentration of 4 g L^{-1} for optimal performance.

5. Availability of data and materials

The data that support the findings of this study are available from the corresponding author, [H.L.], upon reasonable request.".

Declaration of Competing Interest

The authors declare that they have no known competing financial interests or personal relationships that could have appeared to influence the work reported in this paper.

Acknowledgements

"The authors would like to thank the Deanship of Scientific Research at Umm Al-Qura University for supporting this work by Grant Code: 22UQU4131201DSR01"

References

Abdallah, M., Altass, H.M., Al-Gorair, A.S., Al-Fahemi, J.H., Jahdaly, B., Soliman, K.A., 2021. Natural nutmeg oil as a green corrosion inhibitor for carbon steel in 1.0 M HCl solution: chemical, electrochemical, and computational methods. J. Mol. Liq. 323, 115036.

Abdel-Gaber, A.M., Abd-El-Nabey, B.A., Sidahmed, I.M., El-Zayady, A.M., Saadawy, M., 2006. Inhibitive action of some plant extracts on the corrosion of steel in acidic media. Corros. Sci. 48, 2765–2779.

Ahamad, I., Prasad, R., Quraishi, M.A., 2010. Thermodynamic, electrochemical and quantum chemical investigation of some Schiff bases as corrosion inhibitors for mild steel in hydrochloric acid solutions. Corros. Sci. 52, 933–942.

Ashassi-Sorkhabi, H., Asghari, E., 2008. Effect of hydrodynamic conditions on the inhibition performance of l-methionine as a "green" inhibitor. Electrochimica Acta 54, 162–167.

Bahlakeh, G., Ramezanzadeh, B., Dehghani, A., Ramezanzadeh, M., 2019. Novel cost-effective and high-performance green inhibitor based on aqueous Peganum harmala seed extract for mild steel corrosion in HCl solution: detailed experimental and electronic/atomic level computational explorations. J. Mol. Liq. 283, 174–195.

Bahrami, M.J., Shahidi, M., Hosseini, S.M.A., 2014. Comparison of electrochemical current noise signals arising from symmetrical and asymmetrical electrodes made of Al alloys at different pH values using statistical and wavelet analysis. Part I: neutral and acidic solutions. Electrochimica Acta 148, 127–144.

Benmahammed, I., Douadi, T., Issaadi, S., Al-Noaimi, M., Chafaa, S., 2020. Heterocyclic Schiff bases as corrosion inhibitors for carbon steel in 1 M HCl solution: hydrodynamic and synergetic effect. J. Dispers. Sci. Technol. 41, 1002–1021.

Bentrah, H., Rahali, Y., Chala, A., 2014. Gum Arabic as an eco-friendly inhibitor for API 5L X42 pipeline steel in HCl medium. Corros. Sci. 82, 426–431.

Berrissoul, A., Ouarhach, A., Benhiba, F., Romane, A., Zarrouk, A., Guenbour, A., Dikici, B., Dafali, A., 2020. Evaluation of Lavandula mairei extract as green inhibitor for mild steel corrosion in 1 M HCl solution. Experimental and theoretical approach. J. Mol. Liq. 313, 113493.

Bertocci, U., Huet, F., Nogueira, R.P., Rousseau, P., 2002. Drift removal procedures in the analysis of electrochemical noise. Corrosion 58, 337–347.

Chafiq, M., Chaouiki, A., Lgaz, H., Salghi, R., Gaonkar, S.L., Bhat, K.S., Marzouki, R., Ali, I.H., Khan, M.I., Shimizu, H., 2020. Synthesis and corrosion inhibition evaluation of a new schiff base hydrazone for mild steel corrosion in HCl medium: electrochemical, DFT, and molecular dynamics simulations studies. J. Adhes. Sci. Technol. 34, 1283–1314.

Chafiq, M., Thari, F.Z., Lee, H., Chaouiki, A., Salghi, R., Ko, Y.G., Karrouchi, K., Bougrin, K., Ali, I.H., Lgaz, H., 2022. Experimental and first-principles DFT insights into the corrosion protection mechanism of carbon steel in an HCl medium by two thiazolidinedione compounds. Mater. Today Commun. 32,. https://doi.org/10.1016/j.mtcomm.2022.103841 103841.

Chaitra, T.K., Mohana, K.N.S., Tandon, H.C., 2015. Thermodynamic, electrochemical and quantum chemical evaluation of some triazole Schiff bases as mild steel corrosion inhibitors in acid media. J. Mol. Liq. 211, 1026–1038.

Chung, I.-M., Kalaiselvi, K., Sasireka, A., Kim, S.-H., Prabakaran, M., 2018. Anticorrosive property of Spiraea Cantoniensisis extract as an eco-friendly inhibitor on mild steel surface in acid medium. J. Dispers. Sci. Technol.

Chung, I.-M., Hemapriya, V., Kim, S.-H., Ponnusamy, K., Arunadevi, N., Chitra, S., Prabakaran, M., Gopiraman, M., 2021. Liriope platyphylla extract as a green inhibitor for mild steel corrosion in sulfuric acid medium. Chem. Eng. Commun. 208, 72–88.

Cordero, B., Gómez, V., Platero-Prats, A.E., Revés, M., Echeverría, J., Cremades, E., Barragán, F., Alvarez, S., 2008. Covalent radii revisited. Dalton Trans. 2832–2838. https://doi.org/10.1039/B801115J.

Cossi, M., Rega, N., Scalmani, G., Barone, V., 2003. Energies, structures, and electronic properties of molecules in solution with the C-PCM solvation model. J. Comput. Chem. 24, 669–681. https://doi.org/10.1002/jcc.10189.

Cottis, R.A., Al-Awadhi, M.A.A., Al-Mazeedi, H., Turgoose, S., 2001. Measures for the detection of localized corrosion with electrochemical noise. Electrochimica Acta 46, 3665–3674.

Danaee, I., Nikparsa, P., Khosravi-Nikou, M.R., Eskandari, H., Nikmanesh, S., 2019. Density Functional Theory and Electrochemical Noise Analysis of Corrosion Inhibition Behavior of N, N'-bis (1-(3, 5-dihydroxyphenyl) ethylidene) propane-1, 3-diamine on Steel in HCl Solution. Prot. Met. Phys. Chem. Surf. 55, 1001–1014.

de Britto Policarpi, E., Spinelli, A., 2020. Application of Hymenaea stigonocarpa fruit shell extract as eco-friendly corrosion inhibitor for steel in sulfuric acid. J. Taiwan Inst. Chem. Eng. 116, 215–222.

Dehghani, A., Bahlakeh, G., Ramezanzadeh, B., Ramezanzadeh, M., 2019a. Electronic/atomic level fundamental theoretical evaluations combined with electrochemical/surface examinations of Tamarindus indiaca aqueous extract as a new green inhibitor for mild steel in acidic solution (HCl 1 M). J. Taiwan Inst. Chem. Eng. 102, 349–377.

Dehghani, A., Bahlakeh, G., Ramezanzadeh, B., Ramezanzadeh, M., 2019b. Potential of Borage flower aqueous extract as an environmentally sustainable corrosion inhibitor for acid corrosion of mild steel: electrochemical and theoretical studies. J. Mol. Liq. 277, 895–911.

Dehghani, A., Bahlakeh, G., Ramezanzadeh, B., Ramezanzadeh, M., 2019c. Detailed macro-/micro-scale exploration of the excellent active corrosion inhibition of a novel environmentally friendly green inhibitor for carbon steel in acidic environments. J. Taiwan Inst. Chem. Eng. 100, 239–261.

Dehghani, A., Bahlakeh, G., Ramezanzadeh, B., Ramezanzadeh, M., 2020a. Potential role of a novel green eco-friendly inhibitor in corrosion inhibition of mild steel in HCl solution: detailed macro/micro-scale experimental and computational explorations. Constr. Build. Mater. 245, 118464.

Dehghani, A., Bahlakeh, G., Ramezanzadeh, B., Ramezanzadeh, M., 2020b. Experimental complemented with microscopic (electronic/atomic)-level modeling explorations of Laurus nobilis extract as green inhibitor for carbon steel in acidic solution. J. Ind. Eng. Chem. 84, 52–71.

Dennington, R., Keith, T.A., Millam, J.M., 2016. GaussView 6.0. 16. Semichem Inc Shawnee Mission KS USA.

Di Virgilio, N., Papazoglou, E.G., Jankauskiene, Z., Di Lonardo, S., Praczyk, M., Wielgusz, K., 2015. The potential of stinging nettle (*Urtica dioica* L.) as a crop with multiple uses. Ind. Crops Prod. 68, 42–49.

Dlouhy, M., Kokalj, A., 2022. How adsorbed H, O, OH, and Cl affect plain adsorption of imidazole on copper. Corros. Sci. 205,. https://doi.org/10.1016/j.corsci.2022.110443 110443.

Ehsani, A., Mahjani, M.G., Hosseini, M., Safari, R., Moshrefi, R., Shiri, H.M., 2017. Evaluation of Thymus vulgaris plant extract as an eco-friendly corrosion inhibitor for stainless steel 304 in acidic solution by means of electrochemical impedance spectroscopy, electrochemical noise analysis and density functional theory. J. Colloid Interface Sci. 490, 444–451.

El Bakri, Y., Guo, L., Essassi, E.M., 2019. Electrochemical, DFT and MD simulation of newly synthesized triazolotriazepine derivatives as corrosion inhibitors for carbon steel in 1 M HCl. J. Mol. Liq. 274, 759–769.

Fadhil, A.A., Khadom, A.A., Fu, C., Liu, H., Mahood, H.B., Mahmoud, A.K., Khalaf, M.Z., Karim, A.M.A., 2020. Ceramics coating materials for corrosion control of crude oil distillation

column: experimental and theoretical studies. Corros. Sci. 162, 108220.
Fawzy, A., Abdallah, M., Zaafarany, I.A., Ahmed, S.A., Althagafi, I. I., 2018. Thermodynamic, kinetic and mechanistic approach to the corrosion inhibition of carbon steel by new synthesized amino acids-based surfactants as green inhibitors in neutral and alkaline aqueous media. J. Mol. Liq. 265, 276–291.
Fernandes, C.M., da Fagundes, T.d.S.F., dos Santos, N.E., Rocha, T. S.d.M., Garrett, R., Borges, R.M., Muricy, G., Valverde, A.L., Ponzio, E.A., 2019a. Ircinia strobilina crude extract as corrosion inhibitor for mild steel in acid medium. Electrochimica Acta 312, 137–148.
Fernandes, C.M., Fagundes, T.D.S.F., dos Santos, N.E., Rocha, T.S. D.M., Garrett, R., Borges, R.M., Muricy, G., Valverde, A.L., Ponzio, E.A., 2019b. Ircinia strobilina crude extract as corrosion inhibitor for mild steel in acid medium. Electrochimica Acta 312, 137–148. https://doi.org/10.1016/j.electacta.2019.04.148.
Frisch, M.J., Trucks, G.W., Schlegel, H.B., Scuseria, G.E., Robb, M. A., Cheeseman, J.R., Scalmani, G., Barone, V., Mennucci, B., Petersson, G.A., 2016. GAUSSIAN09, Gaussian, Inc., Wallingford, CT, USA, (2009). Sample Availab. Samples Compd. 3a–6f Are Available Authors.
Gerengi, H., Uygur, I., Solomon, M., Yildiz, M., Goksu, H., 2016. Evaluation of the inhibitive effect of Diospyros kaki (Persimmon) leaves extract on St37 steel corrosion in acid medium. Sustain. Chem. Pharm. 4, 57–66.
Haddadi, S.A., Alibakhshi, E., Bahlakeh, G., Ramezanzadeh, B., Mahdavian, M., 2019. A detailed atomic level computational and electrochemical exploration of the Juglans regia green fruit shell extract as a sustainable and highly efficient green corrosion inhibitor for mild steel in 3.5 wt% NaCl solution. J. Mol. Liq. 284, 682–699.
Haruna, K., Obot, I.B., Ankah, N.K., Sorour, A.A., Saleh, T.A., 2018. Gelatin: A green corrosion inhibitor for carbon steel in oil well acidizing environment. J. Mol. Liq. 264, 515–525.
Hassanien, A.S., Akl, A.A., 2016a. Effect of Se addition on optical and electrical properties of chalcogenide CdSSe thin films. Superlattices Microstruct. 89, 153–169. https://doi.org/10.1016/j.spmi.2015.10.044.
Hassanien, A.S., Akl, A.A., 2016b. Electrical transport properties and Mott's parameters of chalcogenide cadmium sulphoselenide bulk glasses. J. Non-Cryst. Solids 432, 471–479. https://doi.org/10.1016/j.jnoncrysol.2015.11.007.
Hassanien, A.S., Akl, A.A., 2018. Influence of thermal and compositional variations on conduction mechanisms and localized state density of amorphous Cd50S50−xSex thin films. J. Non-Cryst. Solids 487, 28–36. https://doi.org/10.1016/j.jnoncrysol.2018.02.018.
Hourahine, B., Aradi, B., Blum, V., Bonafé, F., Buccheri, A., Camacho, C., Cevallos, C., Deshaye, M., Dumitrică, T., Dominguez, A., 2020. DFTB+, a software package for efficient approximate density functional theory based atomistic simulations. J. Chem. Phys. 152, 124101.
Izadi, M., Shahrabi, T., Ramezanzadeh, B., 2018. Synthesis and characterization of an advanced layer-by-layer assembled Fe3O4/polyaniline nanoreservoir filled with Nettle extract as a green corrosion protective system. J. Ind. Eng. Chem. 57, 263–274. https://doi.org/10.1016/j.jiec.2017.08.032.
Keramatinia, M., Ramezanzadeh, B., Mahdavian, M., 2019. Green production of bioactive components from herbal origins through one-pot oxidation/polymerization reactions and application as a corrosion inhibitor for mild steel in HCl solution. J. Taiwan Inst. Chem. Eng. 105, 134–149. https://doi.org/10.1016/j.jtice.2019.10.005.
Khadraoui, A., Khelifa, A., Hachama, K., Mehdaoui, R., 2016. Thymus algeriensis extract as a new eco-friendly corrosion inhibitor for 2024 aluminium alloy in 1 M HCl medium. J. Mol. Liq. 214, 293–297.
Khaled, K.F., 2008. Molecular simulation, quantum chemical calculations and electrochemical studies for inhibition of mild steel by triazoles. Electrochimica Acta 53, 3484–3492.
Kokalj, A., 2010. Is the analysis of molecular electronic structure of corrosion inhibitors sufficient to predict the trend of their inhibition performance. Electrochimica Acta 56, 745–755.
Kokalj, A., 2022. Corrosion inhibitors: physisorbed or chemisorbed? Corros. Sci. 196, 109939.
Kokalj, A., Behzadi, H., Farahati, R., 2020. DFT study of aqueous-phase adsorption of cysteine and penicillamine on Fe(110): Role of bond-breaking upon adsorption. Appl. Surf. Sci. 514,. https://doi.org/10.1016/j.apsusc.2020.145896 145896.
Kumar, D., Jain, N., Jain, V., Rai, B., 2020a. Amino acids as copper corrosion inhibitors: A density functional theory approach. Appl. Surf. Sci. 514,. https://doi.org/10.1016/j.apsusc.2020.145905 145905.
Kumar, D., Jain, V., Rai, B., 2020b. Imidazole derivatives as corrosion inhibitors for copper: a DFT and reactive force field study. Corros. Sci. 171, 108724.
Kumar, D., Jain, V., Rai, B., 2022. Capturing the synergistic effects between corrosion inhibitor molecules using density functional theory and ReaxFF simulations-A case for benzyl azide and butyn-1-ol on Cu surface. Corros. Sci. 195, 109960.
Lgaz, H., Lee, H., 2022. First-principles based theoretical investigation of the adsorption of alkanethiols on the iron surface: A DFT-D3 study. J. Mol. Liq. 348,. https://doi.org/10.1016/j.molliq.2021.118071 118071.
Li, W., He, Q., Pei, C., Hou, B., 2007. Experimental and theoretical investigation of the adsorption behaviour of new triazole derivatives as inhibitors for mild steel corrosion in acid media. Electrochimica Acta 52, 6386–6394.
Loganayagi, C., Kamal, C., Sethuraman, M.G., 2014. Opuntiol: an active principle of opuntia elatior as an eco-friendly inhibitor of corrosion of mild steel in acid medium. ACS Sustain. Chem. Eng. 2, 606–613.
Ma, C., Song, S., Gao, Z., Wang, J., Hu, W., Behnamian, Y., Xia, D.-H., 2017. Electrochemical noise monitoring of the atmospheric corrosion of steels: identifying corrosion form using wavelet analysis. Corros. Eng. Sci. Technol. 52, 432–440.
Maizia, R., Dib, A., Thomas, A., Martemianov, S., 2018. Statistical short-time analysis of electrochemical noise generated within a proton exchange membrane fuel cell. J. Solid State Electrochem. 22, 1649–1660.
Mansfeld, F., Sun, Z., Hsu, C.H., 2001. Electrochemical noise analysis (ENA) for active and passive systems in chloride media. Electrochimica Acta 46, 3651–3664.
Markhali, B.P., Naderi, R., Mahdavian, M., Sayebani, M., Arman, S. Y., 2013. Electrochemical impedance spectroscopy and electrochemical noise measurements as tools to evaluate corrosion inhibition of azole compounds on stainless steel in acidic media. Corros. Sci. 75, 269–279.
Mehdipour, M., Ramezanzadeh, B., Arman, S.Y., 2015. Electrochemical noise investigation of Aloe plant extract as green inhibitor on the corrosion of stainless steel in 1 M H_2SO_4. J. Ind. Eng. Chem. 21, 318–327.
Mourya, P., Banerjee, S., Singh, M.M., 2014. Corrosion inhibition of mild steel in acidic solution by Tagetes erecta (Marigold flower) extract as a green inhibitor. Corros. Sci. 85, 352–363.
Özcan, M., Dehri, İ., Erbil, M., 2004. Organic sulphur-containing compounds as corrosion inhibitors for mild steel in acidic media: correlation between inhibition efficiency and chemical structure. Appl. Surf. Sci. 236, 155–164.
Panicker, C.Y., Varghese, H.T., Manjula, P.S., Sarojini, B.K., Narayana, B., War, J.A., Srivastava, S.K., Van Alsenoy, C., Al-Saadi, A.A., 2015. FT-IR, HOMO–LUMO, NBO, MEP analysis and molecular docking study of 3-Methyl-4-{(E)-[4-(methylsulfanyl)-benzylidene] amino} 1H-1, 2, 4-triazole-5 (4H)-thione. Spectrochim. Acta. A. Mol. Biomol. Spectrosc. 151, 198–207.

Perdew, J.P., Burke, K., Ernzerhof, M., 1996. Generalized gradient approximation made simple. Phys. Rev. Lett. 77, 3865.

Quraishi, M.A., Singh, A., Singh, V.K., Yadav, D.K., Singh, A.K., 2010. Green approach to corrosion inhibition of mild steel in hydrochloric acid and sulphuric acid solutions by the extract of Murraya koenigii leaves. Mater. Chem. Phys. 122, 114–122.

Rabizadeh, T., Asl, S.K., 2019. Casein as a natural protein to inhibit the corrosion of mild steel in HCl solution. J. Mol. Liq. 276, 694–704.

Rajput, P., Chaudhary, M., Sharma, R.A., 2018. Phytochemical and pharmacological importance of genus Urtica-a review. Int J Pharm Sci Res 9, 1387–1396.

Ramezanzadeh, B., Arman, S.Y., Mehdipour, M., Markhali, B.P., 2014. Analysis of electrochemical noise (ECN) data in time and frequency domain for comparison corrosion inhibition of some azole compounds on Cu in 1.0 M H2SO4 solution. Appl. Surf. Sci. 289, 129–140.

Saeed, M.T., Saleem, M., Usmani, S., Malik, I.A., Al-Shammari, F.A., Deen, K.M., 2019. Corrosion inhibition of mild steel in 1 M HCl by sweet melon peel extract. J. King Saud Univ.-Sci. 31, 1344–1351.

Salmasifar, A., Edraki, M., Alibakhshi, E., Ramezanzadeh, B., Bahlakeh, G., 2021. Combined electrochemical/surface investigations and computer modeling of the aquatic Artichoke extract molecules corrosion inhibition properties on the mild steel surface immersed in the acidic medium. J. Mol. Liq. 327, 114856.

Saxena, A., Prasad, D., Haldhar, R., Singh, G., Kumar, A., 2018. Use of Saraca ashoka extract as green corrosion inhibitor for mild steel in 0.5 M H_2SO_4. J. Mol. Liq. 258, 89–97.

Sedik, A., Lerari, D., Salci, A., Athmani, S., Bachari, K., Gecibesler, İ., Solmaz, R., 2020. Dardagan Fruit extract as eco-friendly corrosion inhibitor for mild steel in 1 M HCl: electrochemical and surface morphological studies. J. Taiwan Inst. Chem. Eng. 107, 189–200.

Shahidi, M., Jafari, A.H., Hosseini, S.M.A., 2012. Comparison of symmetrical and asymmetrical cells by statistical and wavelet analysis of electrochemical noise data. Corrosion 68, 1003–1014.

Shi, Y., Zhang, Z., Su, J., Cao, F., Zhang, J., 2006. Electrochemical noise study on 2024–T3 Aluminum alloy corrosion in simulated acid rain under cyclic wet–dry condition. Electrochimica Acta 51, 4977–4986.

Singh, A., Ansari, K.R., Chauhan, D.S., Quraishi, M.A., Lgaz, H., Chung, I.-M., 2020. Comprehensive investigation of steel corrosion inhibition at macro/micro level by ecofriendly green corrosion inhibitor in 15% HCl medium. J. Colloid Interface Sci. 560, 225–236.

Takano, Y., Houk, K.N., 2005. Benchmarking the Conductor-like Polarizable Continuum Model (CPCM) for aqueous solvation free energies of neutral and ionic organic molecules. J. Chem. Theory Comput. 1, 70–77. https://doi.org/10.1021/ct049977a.

Tan, B., Xiang, B., Zhang, S., Qiang, Y., Xu, L., Chen, S., He, J., 2021. Papaya leaves extract as a novel eco-friendly corrosion inhibitor for Cu in H_2SO_4 medium. J. Colloid Interface Sci. 582, 918–931.

Tehrani, M.E.H.N., Ghahremani, P., Ramezanzadeh, M., Bahlakeh, G., Ramezanzadeh, B., 2021. Theoretical and experimental assessment of a green corrosion inhibitor extracted from Malva sylvestris. J. Environ. Chem. Eng. 9, 105256.

Thomas, A.G., Jackman, M.J., Wagstaffe, M., Radtke, H., Syres, K., Adell, J., Lévy, A., Martsinovich, N., 2014. Adsorption Studies of p-Aminobenzoic Acid on the Anatase TiO_2(101) Surface. Langmuir 30, 12306–12314. https://doi.org/10.1021/la5032619.

Verma, C., Ebenso, E.E., Quraishi, M.A., 2017a. Corrosion inhibitors for ferrous and non-ferrous metals and alloys in ionic sodium chloride solutions: a review. J. Mol. Liq. 248, 927–942.

Verma, C., Ebenso, E.E., Quraishi, M.A., 2017b. Ionic liquids as green and sustainable corrosion inhibitors for metals and alloys: an overview. J. Mol. Liq. 233, 403–414.

Verma, C., Ebenso, E.E., Bahadur, I., Quraishi, M.A., 2018. An overview on plant extracts as environmental sustainable and green corrosion inhibitors for metals and alloys in aggressive corrosive media. J. Mol. Liq. 266, 577–590.

Xavier Stango, S.A., Vijayalakshmi, U., 2018. Studies on corrosion inhibitory effect and adsorption behavior of waste materials on mild steel in acidic medium. J. Asian Ceram. Soc. 6, 20–29.

Yeganeh, M., Khosravi-Bigdeli, I., Eskandari, M., Alavi Zaree, S.R., 2020. Corrosion inhibition of l-methionine amino acid as a green corrosion inhibitor for stainless steel in the H2SO4 solution. J. Mater. Eng. Perform. 29, 3983–3994.

Zaabar, A., Aitout, R., Makhloufi, L., Belhamel, K., Saidani, B., 2014. Inhibition of acid corrosion of mild steel by aqueous nettle extracts. Pigment Resin Technol.

Zaabar, A., Aitout, R., Amoura, D., Maizia, R., Makhloufi, L., Saidani, B., 2019. Effect of nettle plant extract on the overconsumption diminution of zinc as sacrificial metal during cementation of copper. Miner. Eng. 142, 105933.

Zaabar, A., Aitout, R., Amoura, D., Maizia, R., Abdesselam, D.A., Makhloufi, L., Saidani, B., 2021. OAT Extract as a Natural Corrosion Inhibitor for Mild Steel in 3% NaCl Solution. Surf. Rev. Lett. 28, 2150084.

Zhang, S.Q., Zhao, H.Y., Shu, F.Y., Wang, G.D., Liu, B., Xu, B.S., 2018. Study on the corrosion behavior of steel Q315NS heat-affected zone in a HCl solution using electrochemical noise. RSC Adv. 8, 454–463.